DEVELOPMENT OF IN-SITU THERMAL MONITORING SYSTEM FOR SELECTIVE LASER SINTERING TO EVALUATE NESTING DESIGN

by

DEHA ÜNAL

Submitted to the Graduate School of Engineering and Natural Sciences

in partial fulfillment of

the requirements for the degree of

Master of Science

Sabancı University

August 2020

DEVELOPMENT OF IN-SITU THERMAL MONITORING SYSTEM FOR SELECTIVE LASER SINTERING TO EVALUATE NESTING DESIGN

APPROVED BY:

Asst. Prof. Dr. Murat Büyük
(Thesis Supervisor) .....

Prof. Dr. Bahattin Koç .....

Prof. Dr. İsmail Lazoğlu .....

DATE OF APPROVAL: 18.08.2020

ABSTRACT

DEVELOPMENT OF IN-SITU THERMAL MONITORING SYSTEM FOR SELECTIVE LASER SINTERING TO EVALUATE NESTING DESIGN

DEHA ÜNAL

Manufacturing Engineering, M.Sc. Thesis, August 2020

Thesis Advisor: Asst. Prof. Dr. Murat Büyük

Keywords: Additive Manufacturing, Selective Laser Sintering, Thermal Monitoring, Process Monitoring, Glass-filled Polyamide 12, Nesting, DSC Analysis

Selective Laser Sintering (SLS) technique is an additive manufacturing process that enables the production of parts using thermoplastic powder raw material. SLS method is preferred in many sectors for the production of functional prototypes and when low number of end-use products are desired. In this process, where the interaction of thermoplastic powder raw material with temperature is very important, a lot of information about the process and the part can be obtained by thermal imaging. In some previous studies, the effects of process parameters and part geometry on process temperatures have been examined. However, the effects of the distance between the parts used in the production plan on the powder and the parts in production have not been studied extensively. To answer that need, in this thesis, the temperatures of the parts in the process were measured by using thermal imaging; bending tests and DSC tests of polyamide 12 (PA12) with glass spheres were carried out. Unlike thermal imaging systems used in previous studies, a new in-situ measurement system was developed that can be used without disrupting the structure of the SLS machine. It was observed that the distance between the parts as a function of the wall thickness of the part, effect the properties of the powder and the part itself.

ÖZET

SEÇİCİ LAZER İLE SİNTERLEME (SLS) YÖNTEMİNDE ÜRETİM PLANI TASARIMINI DEĞERLENDİRMEYE YÖNELİK İN SİTU TERMAL GÖRÜNTÜLEME SİSTEMİ GELİŞTİRİLMESİ

DEHA ÜNAL

İmalat Mühendisliği, Yüksek Lisans Tezi, Ağustos 2020

Tez Danışmanı: Dr. Öğr. Üyesi Murat Büyük

Anahtar Kelimeler: Eklemeli Imalat, Seçici Lazer ile Sinterleme, Termal Görüntüleme, Proses Görüntüleme, Cam Kürecik Katkılı Poliamid 12, DSC Analizi

Seçici Lazer ile Sinterleme (SLS) tekniği, termoplastik toz hammadde kullanılarak parçaların üretilmesini sağlayan bir eklemeli imalat yöntemidir. SLS yöntemi birçok sektörde fonksiyonel prototiplerin ve düşük sayıda son kullanım ürünlerinin üretilmesi amacıyla tercih edilmektedir. Termoplastik toz hammaddenin sıcaklık ile etkileşiminin oldukça önemli olduğu bu proseste termal görüntüleme ile proses ve parça hakkında birçok bilgi elde edilebilmektedir. Daha önce yapılan bazı çalışmalarda proses parametrelerinin ve parça geometrisinin proses sıcaklıklarına etkileri incelenmiştir. Fakat üretim planında kullanılan parçalar arası mesafenin üretimdeki toza ve parçaya etkileri detaylıca incelenmemiştir. Bu gereksinimi karşılamak amacıyla bu tez çalışmasında termal görüntüleme kullanılarak parçaların prosesteki sıcaklıkları ölçülmüştür; cam kürecik katkılı poliamid 12 (PA12)'den üretilen parçalara eğme testi ve üretimden çıkan sinterlenmemiş toza DSC testi yapılmıştır. Daha önceki çalışmalarda kullanılan termal görüntüleme sistemlerinin aksine, SLS makinesinin yapısını bozmadan kullanılabilecek yeni bir sistem geliştirilmiştir. Parçalar arasındaki mesafenin, parçanın duvar kalınlığına bağımlı bir şekilde üretimden çıkan tozun ve parçanın özelliklerinde değişimlere sebep olduğu gözlemlenmiştir.

To my loving family for their infinite support,

and my dear fiance Esra for her support at all time…

ACKNOWLEDGEMENTS

This thesis is a project supported by the Arçelik A.Ş. Research and Development Center.

I would like to thank to;

- Asst. Prof. Dr. Murat Büyük, who is advisor to my master's thesis, for his positive comments and suggestions,
- Arçelik A.Ş. Garage & Maker Lab. manager Mr. Celal Vatansever for his endless support and sharing his expertise and knowledge,
- Mr. Ersin Dönmez for his valuable ideas and studies,
- Materials R&D Department for sharing their expertise and providing testing opportunity,
- Mrs. Şefika Çavuş from Arçelik Eskişehir Plant Plastic Laboratory for her valuable support,
- Enes İnanç, İbrahim Güzel and Ogün Hızar for their valuable ideas.

TABLE OF CONTENTS

LIST OF FIGURES

LIST OF TABLES

ABBREVIATIONS

AM	Additive Manufacturing
SLS	Selective Laser Sintering
CAD	Computer Aided Design
DSC	Differential Scanning Calorimetry
PBF	Powder Bed Fusion
FDM	Fused Deposition Modeling
DED	Direct Energy Deposition
SLA	Stereolithography Apparatus
IRS	Integrated Recycling Station
STL	Stereolithography
MJF	Multi Jet Fusion
ND	Nesting Density
A_{bp}	Area of the build plate
Z_{hp}	Z position of the highest part
PA12	Polyamide 12
IR	Infrared
P_L	Laser Power
V_L	Laser scanning speed
d_L	Laser overlap
TPE	Thermoplastic Elastomer
$T_m°$	Equilibrium melting point
T_C	Crystallization temperature
GPC	Gel Permeation Chromatography

MFR	Melt Flow Rate
ΔH_f	Enthalpy of fusion
ΔH_c	Enthalpy of crystallization
T_m	Melting temperature
LWIR	Long-Wave Infrared
MWIR	Mid-Wave Infrared
HFOV	Horizontal Field of View
AR	Anti-Reflective
ZnSe	Zinc Selenide
LAMPS	Laser Additive Manufacturing Pilot System
ID	Inter-part distance specimen
WT	Wall thickness specimen
ROI	Region of interest
TIFF	Tagged Image File Format
UTM	Universal Testing Machine

CHAPTER 1 INTRODUCTION

1.1. Motivation

Selective Laser Sintering (SLS) process is an additive manufacturing (AM) technology used in the production of; customized parts, functional end-products and prototypes by processing thermoplastic materials. The process's ability to produce batches enables multiple parts to be produced at lower cost and faster times than other AM techniques. Due to the fact that SLS is a thermal process, a lot of information about the process and the resulting part can be obtained by monitoring the temperature distribution in the layers. Some of the new commercially available SLS machines have thermal monitoring systems integrated into the machine to provide sustainable and controllable production. However, for machines that do not have this feature, the integration of the thermal camera into the machine has been made possible by making some permanent changes to the machine [1–3]. Some researchers have also developed SLS system for process monitoring [1]. In this thesis, an innovative thermal monitoring kit that will not require any modification on the machine has been developed and installed without any major modifications to the machine tool structure.

In some previous studies, thermal process monitoring was used to detect the errors during the process[2], to provide automated laser control [3] and to examine the effects of process temperatures on the mechanical properties [4]. In the production planning of the SLS method, the parameters of nesting the parts in the production space significantly affect the production time and cost.

In this thesis, the effects of distances between the parts during the production was monitored with different wall thicknesses, as the placement parameters of the adjacent parts. This production was recorded in real time simultaneously with a thermal camera.

It was aimed to examine the effects of the above-mentioned variables on the non-sintered powder between the parts and the mechanical properties of the sintered part. The effects of distance between parts and wall thicknesses of the adjacent parts on the process temperature was observed and the relationship between the temperature history and the change in the material properties were examined.

1.2. Outline of Thesis

The studies conducted within the scope of the thesis are organized as follows. Chapter 1 includes; motivation, outline and objectives of this thesis. Chapter 2 gives the main theoretical background for additive manufacturing, selective laser sintering process steps, materials for SLS, chemical structure of polyamide 12 and characterization methods for polyamide 12 powder. The literature review of the process monitoring systems, the details of the equipment used in the system that we developed and the development stages of the thermal imaging system are given in Chapter 3. The literature review for the interpretation of the data collected in thermal monitoring systems, the examination and evaluation of the first production recorded with our the originally developed in-situ measurement system, the experimental design in line with the constraints of the measurement system, the processing and evaluation of the images recorded in production through MATLAB are explained in the Chapter 4. Information about the experimental production, procedures for DSC analysis, procedures for three-point bending test, analysis of the results for thermographic measurements, bending test results and DSC analysis results are explained in Chapter 5. The discussion of the results are outlined in Chapter 5. In Chapter 6, the conclusions of this study are given, and in Chapter 7, future research plans are mentioned.

1.3. Objectives

By utilizing process monitoring, production systems are digitalized, so sustainable product quality can be achieved with lower production costs and times. In this thesis, it is aimed to develop an original, add-on open architecture, in-situ thermal monitoring kit that can be placed in the production chamber without modifying the SLS machine. It is attempted to examine the effects of the distance between the sintered parts on the chemical, thermal and mechanical properties of the composite PA12 material and to relate these properties with the temperature data monitored during the process in real time.

CHAPTER 2 THEORETICAL BACKGROUND

During the last decade, additive manufacturing (AM) processes are one of the most promising and developing technologies [5]. Parts are made by successively adding material in layers. Each layer has a finite thickness determined by the special requirements. Specifically, the layer is a cross-section of the part received from the CAD data [6].

Mostly, AM technologies are used to step-up the product development with customized products and increased manufacturing felixibility [7]. Differing from conventional processes, AM technologies can produce geometrically complex parts without tooling [8].

Some of the most common AM technologies are; FDM (Fused Deposition Modeling), SLS (Selective Laser Sintering), DED (Direct Energy Deposition), SLA (Stereolithography Apparatus). All of these stated technologies act in different manner and utilizes different materials; thereby each of them are used for different applications [8].

2.1. Selective Laser Sintering Process

Selective Laser Sintering(SLS) is an additive manufacturing process which belongs to Powder Bed Fusion Processes(PBF) technology group. Essentially, as the name indicates, PBF process includes generating fusion between powder particles laying on the powder bed by using a heat source as illustrated in Figure 1 [9]. SLS is the first commercialized PBF process which uses high intensity collimated beam of energy, a laser beam [6]. Selective Laser Sintering is an important AM technology, which enables the batch production of the parts with polymer materials [10].

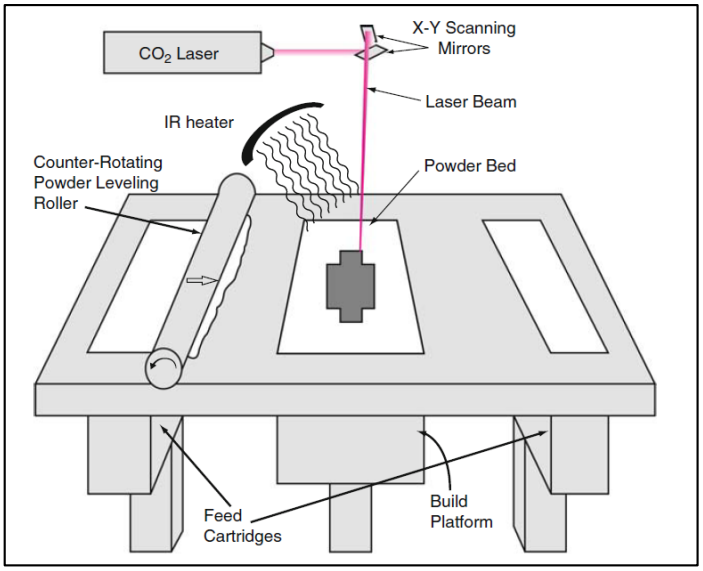

Figure 1 Schematic of Powder Bed Fusion Process [6]

In this thesis, "DTM Sinterstation 2500 Plus" SLS machine was used for the experimental studies. Among the SLS machines, the powder feeding concept and heating system can be changed on different machines but the process chain discussed in the following are general for Selective Laser Sintering process.

2.1.1. Powder Preparation

The preparation for SLS process starts with an essential operation, which is properly arranging the powder mixture. It is a vital procedure for both part quality and manufacturing cost[10].

The SLS powder can be found in three different conditions; virgin powder, overflow powder and used powder. "Virgin" is a pure, unused powder condition. While the roller is laying the powder on the production plate, the excess powder in front of the roller, which called overflow powder falls is into overflow cartridge (Figure 1). Used powder represents the partially degraded, un-sintered powder in a part cylinder which is exposed to temperatures near the melting point of the powder. At the end of a build, more than 90% of the part cylinder content is un-sintered powder [11]. After unpacking the build

cake, some of the used powder aggregates becomes a lump form together. These aggregates should be discharged from the SLS powder cycle.

The feedstock powder for SLS is the blend of virgin, used and overflow powders with different ratios. Preparing the powder blend is a challenge and the blending ratios can be different before each build [10]. The need for blending used powder with virgin and overflow powders is required to avoid powder waste due to the environmental and financial reasons. The virgin ratio of the blend can be different based on the manufacturer and change in a range of 30% to 50% [11]. The used powder ratio is often 50% to 70% and the remaining constitutes for the overflow powder [10] .

Figure 2 Powder aggregates from the build cake [10]

Powder mixing operations can be done either automatically or manually. Primary operation for manual blending is sieving the overflow and used powder. This is required to separate undesired aggregates and possible broken parts from the powder blend. Thereafter, sieved powders and virgin powder are poured into the mixer and left for mixing few hours to achieve homogenous blend. Well-ventilated environment and personal protective equipment are needed due to the risk of spilling of powder while transferring for the manual preparation. There are automated powder recycling solutions such as 3D Systems Integrated Recycling System (IRS). This automated pneumatic-driven system has its own powder bins for virgin, used and blended powder. The IRS enables reciprocal transfer of the powder through hoses to the SLS machine. This closed-loop powder recycling unit helps to prevent direct contact with the powder. IRS blends the powder corresponding to the blending ratio pre-defined by the user and conveys the blended powder back to the SLS machine. Even though automated powder preparation

systems make the operation easier, each build could have different build height, nesting density and build time. These parameters directly affect the condition of the used powder. Therefore, there is a need for controlling the used powder after each build.

2.1.2. STL Data Preparation

In AM technology, nearly all machines accept the STL data. According to ASTM F2792-12a, "It is the file format for 3D model data used by machines to build physical parts; STL is the de facto standard interface for additive manufacturing systems. STL is originated from the term Stereolithography" (pp. 3). It is important to note that the aim of the STL data is representing the geometry for AM machines [12].

Designing of the part model needs Computer Aided Design (CAD) software. It is necessary to consider AM rules for design during the designing stage. The completed CAD data can be converted to STL file format from the CAD software automatically as illustrated in Figure 3 [6]. It is often possible to have problems during the conversion. Even though the build job preparing software "Build Setup" of DTM Sinterstation 2500 Plus has the automatic repairing tool, some of the failures cannot be fixed automatically. Therefore, STL data of the model must be controlled before preparing the build job. There are different software tools for detecting and repairing the failures. "Magics" software from the Materialise Company is one of the most common tools.

Figure 3 CAD model is in the left, STL format on the right

STL format uses mesh of triangles to represent the surfaces to be built. The resolution of the triangles directly affects the quality of the part as illustrated in Figure 4 [10]. The size of the smallest triangle on STL format have to be smaller than the resolution of the AM machine [13].

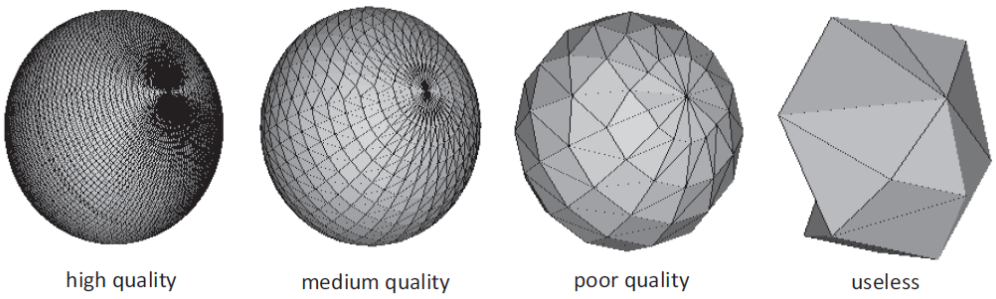

Figure 4 Representation of circles with different triangle mesh resolutions

2.1.3. Build Job Preparation

The most advantageous aspect of SLS process is that, there is no need for support elements for the parts. The powder bed itself acts like a mold and support the parts. This enables to build all parts together freely packed in the build space. In the last few years, newly emerged AM technology Multi Jet Fusion (MJF) has no need for support structures, which also permits packing parts all together [14].

There are two main reasons that makes the build job preparation important. These are; process limitations and the process productivity. For SLS process there are some important rules to consider while planning the build packet. These rules are established from process limitations. Machine manufacturers has their guidelines to lead users on the right way. It needs a lot of experience and know-how to perform a smooth operation, where some vital ones are discussed in this Chapter.

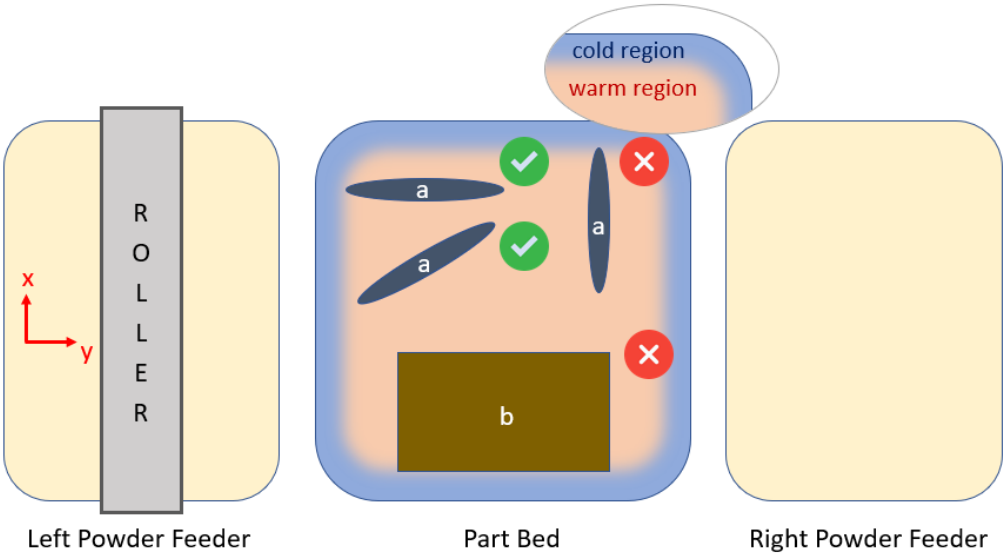

Figure 5 Schematic of top view from SLS machine

The build preparation includes two stages. It starts with orienting each part with respect to build volume coordinate system. The following rules should be considered while deciding on the orientation:

- As the roller moves along y-axis, the longitudinal side of the tall parts shouldn't be vertical to rollers' moving direction like the part named "a" in Figure 5. If so, it is possible that roller can sweep away the part from longitudinal edge.
- Large cross-sectional areas never be placed completely flat on the build volume. Long time of laser scanning will cause overheating. It is important to check distribution of the cross-sectional area of the part along z-axis. If the part is like the "b" in Figure 5, it should be rotated around x-axis or y-axis to decrease the area.

After orientation of each part is completed, the last step is the nesting operation. Nesting is an essential operation for SLS process. For each build process; the resulting build time, cooling time, powder deterioration rate and build errors can be directly related with the nesting design. The main function of nesting is to pack large batches of parts as much as possible with the lowest build height. There are commercial softwares for nesting the parts. Materialise Magics software has special add-on called "Sinter Module". This add-on enables 3D-Nesting of the parts within the build space while allowing the user to define parameters for nesting. The efficiency of nested batch can be measured by nesting density (ND);

$$ND = \frac{\sum Volume_{all\ parts}}{A_{bp}\, x\, Z_{hp}}\ x\, 100\% \qquad \text{(Equation 1)}$$

Where, A_{bp} and Z_{hp} are the area of the build plate and z-position of the highest part, respectively [15]. It is desired to have highest nesting density to minimize the cost of the parts. For the same batch of parts, nesting density can only increase with a reduction in the build height. The minimum distance between the parts should be as low as possible to increase nesting density. As a consequence of higher density, the risk of failure increases. In SLS process, freely distributed powder exists between each part and moving the parts closer to each other causes the risk of fusing different parts together.

Each slice of the build job should contain at least one sintering location. This is required to prevent thermal gradient between successive layers. Otherwise, warping of the part is unavoidable. Sides of the build space mostly colder than the core region. To avoid thermal gradients on the part, margin to sides of the build space should be predetermined. This determination can be done by thermal imaging. Magics Sinter Module has the option for adjusting "Margin to sides". Increasing the distance to sides will prevent thermal gradients on the parts. However, it will decrease the usable production plate area which increases the build height and reduces the nesting density.

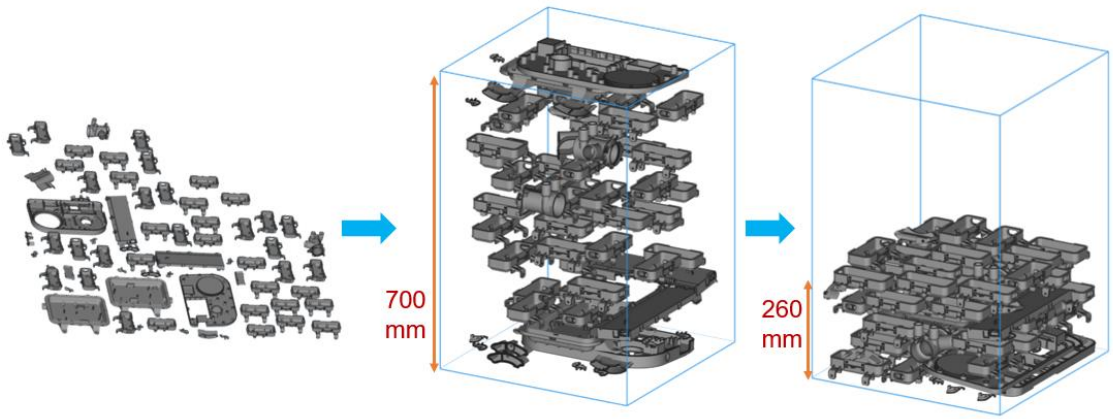

Figure 6 Nesting operation on Magics Sinter Module

In Figure 6, a nesting operation at Magics Sinter Module is illustrated with 70 parts. After starting the nesting process, the algorithm first fits all parts in the build space. This specific example in Figure 6 is given from 3D Systems SPro230 SLS machine configuration. This machine has the maximum z-height of 700 millimeters and roughly nesting the parts can give a result of full machine height. With this build height, the nesting density is 2% and the manufacturing process will be approximately 60 hours. For a significant nesting operation, software should perform a lot of iterations to optimize the nesting density. At the end of the iterations on software, the latest result is obtained as 260 millimeters for build height and 6% nesting density. This latest build pack will take approximately 32 hours. It is also necessary to consider the cool-down stage, which takes as long as the build time. The cool down will be explained in Section 2.2.3.

The nested build pack is lastly transferred to DTM (3D Systems) Build Setup software to prepare electronic build job. Electronic build job consists of STL files and production parameters; part profile, build profile and scale parameters. Part profile comprise

parameters of the laser while sintering the part. These laser parameters are basically; laser power, scanning speed and hatch distance. Build profile includes the parameters of the process; layer thickness, heater parameters, roller parameters. The laser exposure causes powder to melt and solidify. The sintered powder exposes to thermal contraction during this phase transformation and it alters the dimensions. This is an inherent property and inevitable. To overcome this distortion, dimensions of the part has to be scaled in both x, y and z-saxes. Each SLS material, even the blend of the same material has different thermal properties. Due to this variation, scale parameters should be applied to achieve dimensional accuracy of the end product.

2.2. Manufacturing Process

Preliminary preparation of the SLS machine should be done according to machine manufacturers' handbook. There are kind of things such as inspecting some parts of the machine, cleaning the laser window etc. After completing the preparation and loading the blended powder, the door of the system should be closed. Before the process, nitrogen should be applied as protective gas. Then, heaters can be open and process starts [10].

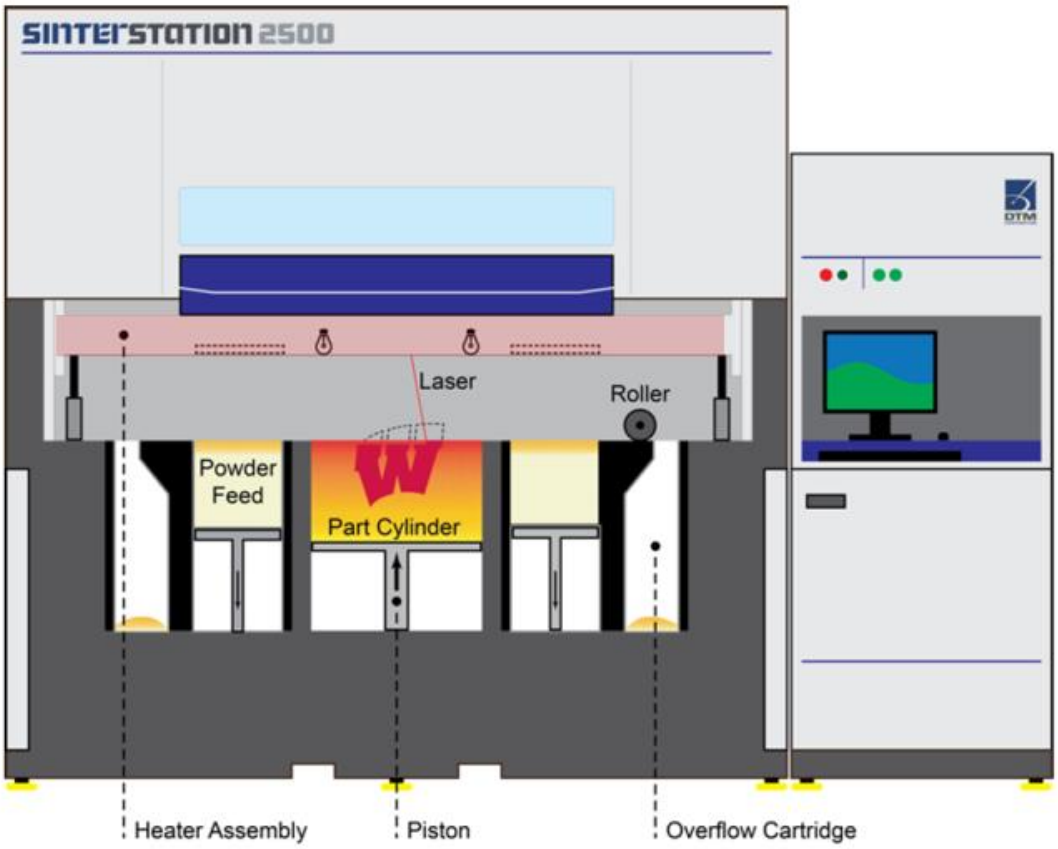

Figure 7 Schematic of DTM Sinterstation 2500 Plus SLS machine

The progression of SLS process is in the sequence of the following;

1. Warm-up Stage
2. Build Stage
3. Cool-down Stage
4. Post-processes

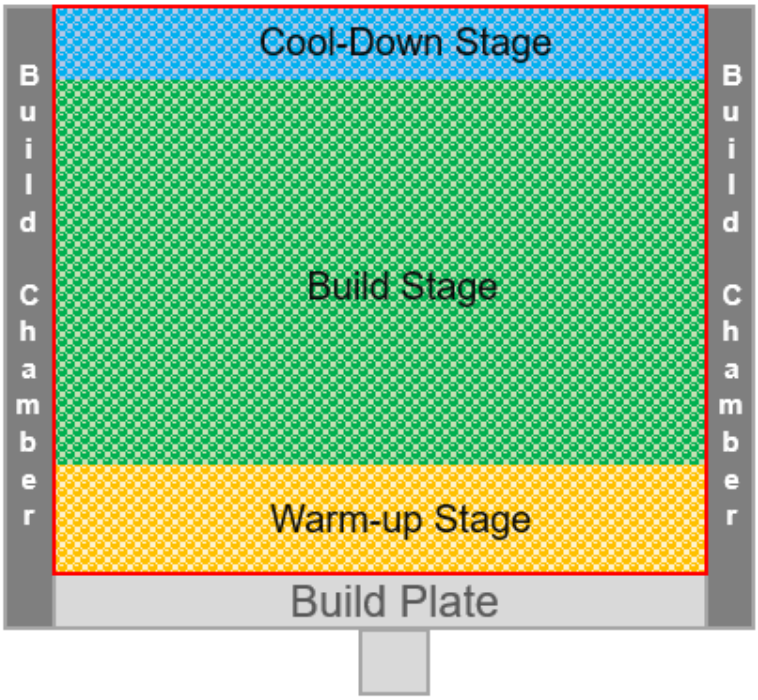

Figure 8 Schematic of stages inside the build space during the SLS process

The red-lined field (Figure 8) is 2D representation of the 3D spatial term, which is "build space". The build space is surrounded with the build chamber and the build plate. Each of the surroundings has its' separately controlled heater systems. The top three stages occur in the build space and the place of each stage is shown in Figure 8 with different colors.

2.2.1. Warm-Up Stage

The main concern during the SLS process is controlling the heat distribution homogenously and conforming the part bed temperature in the desired range for each successive layer. Before the laser sintering begin, warm up stage takes place to ensure thermally stable powder base. During the warm-up stage, roller just add layers of powder consecutively without laser sintering any powder. This stage continues till the powder achieve the predetermined temperature in a controlled manner. This also acts as a barrier for heat transfer towards the build plate.

For a PA12-based powder material, the powder bed is heated up approximately to 175°C. In order to selectively melt the powder, remaining 20-25°C temperature is provided by exposing to laser energy. As can be seen, the majority of the heat exists in the powder bed prior to the laser exposure.

The powder bed heating source on SLS process is located above the powder beds. In a DTM2500 SLS machine, there are 3 radiant heaters. Two of these are placed above the left and right powder feeders, and the third is placed above the part bed. The important stage of powder heating takes place prior to sintering the part bed. If the powder on the part bed is heated less than the required temperature, this will cause curling; if it is heated higher than required temperature, this will cause more scrap powder and hard to break off from the part. To control the powder bed temperature, there are IR sensors behind the feeders and powder bed. The radiant heaters heat the powder by using radiation. Most of the radiation is absorbed by the powder itself and the remaining wastes by reflection. Accordingly, to heat up the powder bed to 175°C, the heaters' own temperature has to reach more than 200°C. In theory, while the heating procedure of the process is as has just been described, in practice there are many uncertainties and instability.

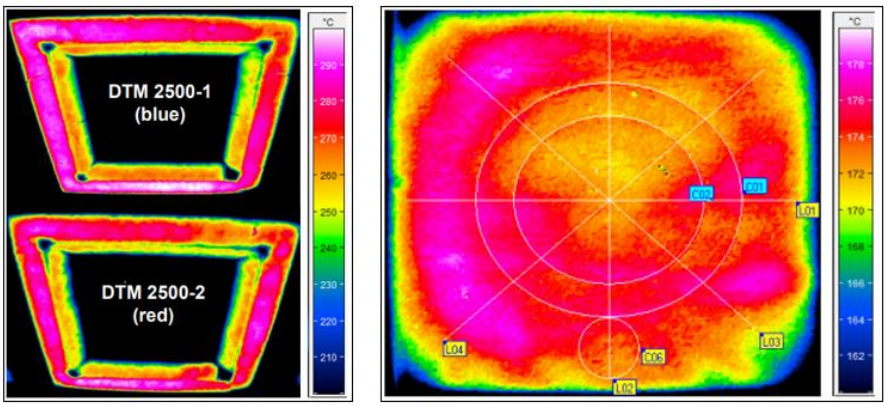

Figure 9 Thermal imaging of; radiant part bed heaters(left), part bed surface(right) [16]

Temperature distribution on the part bed heater is not homogeneous in a DTM2500 machine. Thermal imaging is necessary to inspect heating performance. Wegner and Witt showed this uneven distribution with IR camera measurements (Figure 9). They also validated this uneven part bed heater performance changes with another DTM2500 machine. The uneven distribution of temperature on the heater directly causes inhomogeneous heat distribution on the part bed. This causes partially curling parts in-process, mechanical property gradients on the same part and non-repeatability[16].

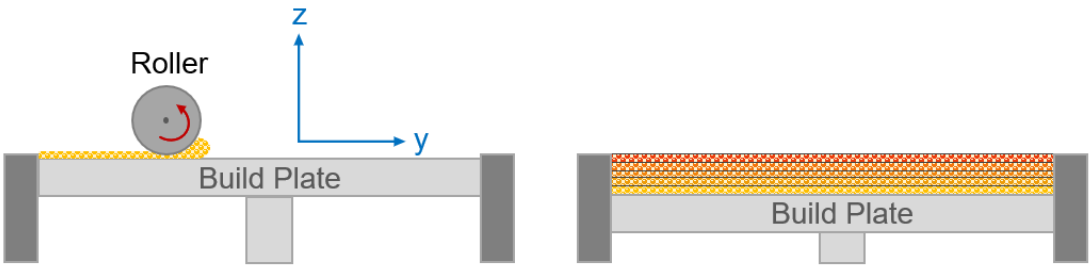

Figure 10 Powder laying process

Before the roller start to lay the powder, build plate moves downward as the layer thickness height. While the roller moves back and forth on y-axis, it rotates always opposite to the motion on y-axis. This counter rotation is applied to avoid layer shifts and process errors due to over-compression on powder bed.

Warm-up stage usually completes in few hours and it is expected to achieve required thermal barrier against downward cooling and intended powder bed temperature[17].

2.2.2. Build Stage

The selective laser sintering process starts with the build stage. Build stage is where the powder particles selectively sintered by laser exposure. The thermoplastic polymer powder subjected to heat and its temperature kept 10-15°C below the materials melting temperature. This high temperature is required to ensure that there is minimum thermal gradient on the part bed and parts warping [18]. It is necessary to maintain build space temperature higher than the materials' crystallization temperature. If not, the quick crystallization happens and warping of the sintered part appears [10]. Both sintered powder and the un-sintered powder are subjected to these temperatures. This ensures better coalescence for the sintered part. However, exposing higher temperatures deteriorates mechanical and thermal properties of the powder[11].

The parameters for the SLS process are specified separately for laser and the build chamber. The main laser parameters are; laser power, scan speed, scan spacing. The energy contribution of the laser can be determined by the Andrew number (A_n).

$$A_n = \frac{P_L}{v_L \ x \ d_L} \left(\frac{J}{mm^2}\right) \qquad \text{(Equation 2)}$$

Where P_L is the laser power in Watts or Joules/second, v_L is the laser scan speed in millimeters/second and d_L is the laser overlap in millimeters (Figure 11). In terms of part quality, lower laser power and laser scan speed is the best choice. However, in terms of economical aspect it is more efficient to continue builds with higher laser scan speeds [10].

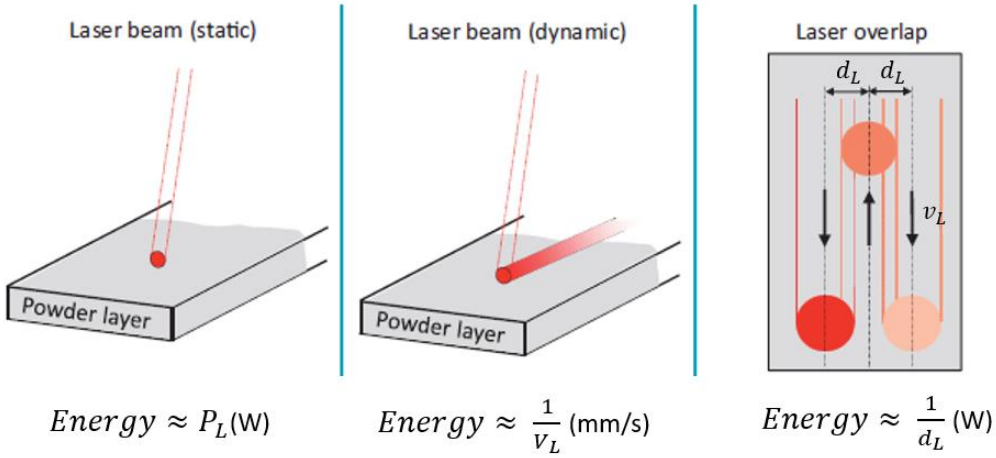

Figure 11 Energy input related with the laser parameters

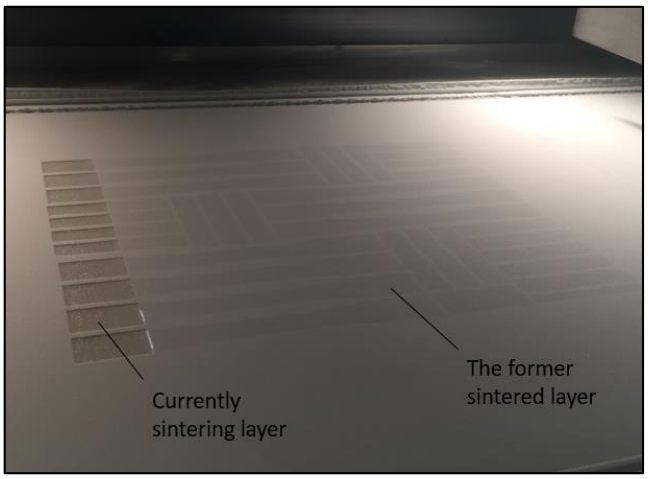

Figure 12 View of the build stage; the former sintered and currently sintering layer [source: Arçelik AŞ]

2.2.3. Cool-Down Stage

Actually, there are two cool-down stages for SLS. As shown in Figure 8, one of them occurs in the manufacturing step. After completing the build stage, to hinder the fast cooling from the top side, roller continues to lay new layers of powder to form a heat

barrier on the powder bed. During this first cool-down stage, heater temperatures gradually decreases to avoid from immediate cooling.

The last cool-down stage is sequent stage of the manufacturing process. Before removing the parts out of the build cake, parts have to be cooled around glass transition temperature of the material. If the parts are removed too hot from the powder cake, the parts may deteriorate due to uncontrolled crystallization. Especially for PA 12 material, significant yellowing may occur in the parts due to oxidation at high temperatures. therefore, parts that have been successfully sintered will be rejected [10].

Figure 13 Cool-down stage at the end of the manufacturing process [source: Arçelik AŞ]

2.2.4. Post-Processing

After the parts are manually removed, they are blasted with compressed air to eliminate loose powder. This is important for possible subsequent post-processing [10]. The parts can then be painted or impregnated with resin to ensure sealing.

2.3. SLS Materials

Polymer materials are divided among themselves as thermoplastic, elastomeric and thermoset. This distinction also affects the production methods and basic properties of polymers.

Thermoplastic materials can be reversibly deformed by heating. Elastomer and thermoset materials do not have the same transformation, melting does not occur in these materials. When examined at the molecular level, the molecular chains of thermoplastics are interconnected by weak secondary valence bonds. With sufficient heat energy supplied, the chains begin to separate from each other and it is observed that the polymer material behaves like a viscous melt. Unlike thermoplastics, it is not possible to dissolve crosslinks under the influence of heat energy if polymer chains are bonded to each other by chemical bonds. There is a special case in thermoplastic elastomer (TPE) materials. Cross-links in TPEs are connected by physical networks instead of covalent bonds. Thermoplastic materials are suitable for processing by laser sintering. Polymer powders are melted by supplying energy by laser radiation. As the laser energy reaches the powder particles, the particles consolidate (Figure 14.b) in the areas it scans and forms the plastic part.

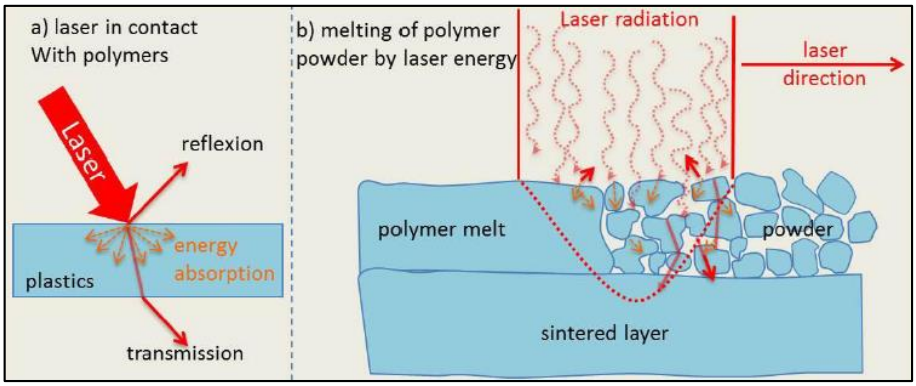

Figure 14 Melting of the powder by laser radiation[19]

The glass transition temperature is a thermodynamically second-order phase change with a transition from solid to solid. So at this temperature, there is no change in the heap condition of the material. It can also be specified as the softening point of amorphous regions of the polymer. Melting point is related to the crystal structure of the polymer. If the arrangement of crystalline molecules or polymer chains begins to dissolve by heating, the polymer material is melting and first-order phase change from solid to liquid takes place [20].

Monomers can be connected to each other to form polymer chains; polymerization can be accomplished by various methods. The most well-known technologies are radical and ionic polymerizations and step growth reactions. In radical and ionic polymerization, each

monomer is added to the end of chain. During the reaction, the end of the chain is highly reactive, within a few seconds the chain structure which started by the monomer is formed. After the polymerization is completed, the end of the chain is passivated by different reactions. Polymers produced in this way do not have active chain ends. In the step growth reaction, the polymer consists of bi-functional or multifunctional monomers. Oligomers are formed initially and then come together to form polymer chains. Due to the nature of this reaction, two different functional end groups can occur in any linear polymer chain at any time of the reaction. Once the reaction is complete, the active chain ends are also products of the reaction [10].

Some thermoplastic materials processed by SLS method are as follows; polyamide 12 (PA12), polyamide 11 PA11), polystyrene (PS), Acrylonitrile Butadiene Styrene (ABS), Polycarbonate (PC), Polylactic Acid (PLA), Polyetherimide (PEI), Polypropylene (PP), Polyetheretherketone (PEEK) and thermoplastic polyurethane [21].

2.3.1. Polyamide

Polyamides, most widely used commercial SLS materials, are step-growth polymers. A water molecule is released at each step of the polyamide synthesis reaction. Thus, the synthesis of polyamide is a polycondensation reaction. These are mostly used unregulated. Reactive chain ends are not hindered by a special termination reaction in polycondensates, which is used unregulated. During production with SLS, machine components and powder material properties can be significantly affected due to post-condensation reactions. Besides the end-chain properties, the chemical structure and thermal properties of the material are also of great importance in terms of laser sinterability [10].

Polyamide 12 consists of a combination of carbon atoms and amide group (COHN). The molecular structure is shown in Figure 15. The presence of the amide group is known to increase chain flexibility in semi-crystalline polymers. Due to the amide group, backbone of PA12 is flexible and long chains of PA12 can transform to chain folded structure by the crystallization process [18].

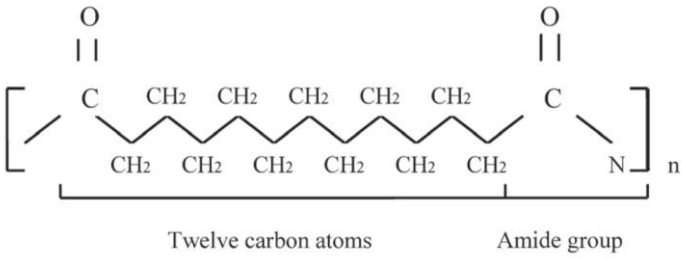

Figure 15 The molecule chain structure of PA12

PA12 is a semi-crystalline polymer. It includes both amorphous and crystalline structure together. Amorphous regions are irregular form of the molecule chains. This region controls the polymer toughness due to its irregular order. Amorphous region is characterized by glass transition temperature. Mechanical properties, elasticity and brittleness, are determined by the crystal structure.

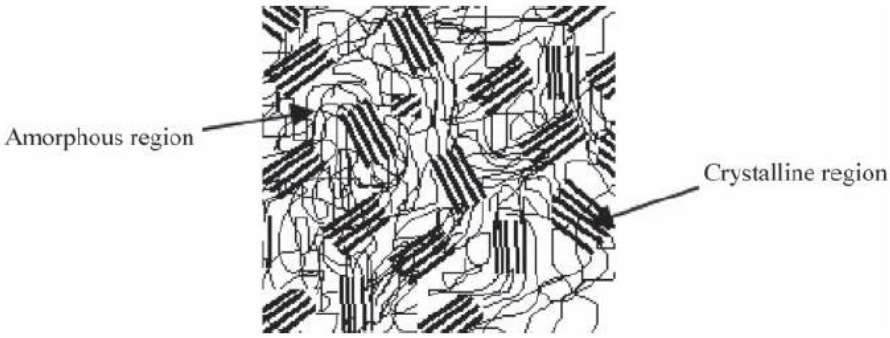

Figure 16 Demonstration of semi-crystalline polymer molecule structure

Crystallization occurs with nucleation and growth stages, respectively. The first phase, nucleation takes place in the amorphous region and starts slightly below the melting temperature. At this stage, the chains are activated by intermolecular forces and arranged in a parallel row. Thus, the polymer melt, which is found in a complex form, forms stable nuclei. During cooling of the melt, the core regions begin to grow with the addition of other chain groups to the nuclei, this behavior constitutes the second phase of crystallization [22].

Degree of supercooling is an important factor which affects the crystallization growth rate. In the following equation; ΔT is the degree of supercooling, $T_m°$ is the equilibrium melting point of a totally crystalline material and Tc, the crystallization temperature of the PA12.

$$\Delta T = T_m{}^o - T_c \qquad \text{(Equation 3)}$$

In the laser sintering process, mobility occurs in PA12 molecules at temperatures higher than the glass transition temperature, this is known as the "Brownian motion". This encourages free radicals to attract more molecules and connect to themselves. The probability of growing molecule chains increases with increasing temperature and time to which powder is exposed. That is, molecules will continue to grow as long as the un-sintered powder in the SLS machine remains inside the machine during production and cooling stage. As a result, the molecular weight and viscosity of PA12 will increase[10].

There are additives that trigger nucleation for polymers. By using these additives, the effects caused by the increased molecular weight of the polymer can be compensated. One of the benefits of these additives is to prevent the delay of crystallization of the material.

Some micron-sized reinforcements are made to improve the mechanical and physical properties of the materials used in laser sintering. These micron-sized reinforcing materials; glass beads, silicon carbide, hydroxyapatite, aluminum powder, carbon nanofibers [23]. Glass reinforcement in thermoplastics is preferred due to increasing load bearing capacity in the elastic deformation range. Glass reinforcement in the form of spheres contributes to increasing the bulk density of the powder and improving the powder flow properties. It is frequently preferred as a reinforcing material because it increases isotropy in the properties of the produced parts and is less affected by thermal distortions after production [14]. Cano et al.[21] observed that the fracture behavior of the glass-bead-reinforced PA12 material was not affected by the production orientation or process temperature.

2.3.2. Material Testing Methods

PA12 material in SLS process waits long periods in the nitrogen atmosphere at temperatures close to the melting point. Meanwhile, post-condensation reactions take place and this significantly affects the recyclability and processability properties of the material. For this reason, GPC, MFR, melt rheology or DSC tests were performed in the literature to examine the changes in the properties of the material.

In the Melt Flow Rate (MFR) test, the molten thermoplastic material is extruded from a capillary mold under certain temperature and load conditions, and the melt flow rate is measured. As a result of this measurement, interpretation can be made about the viscosity of the material. The flowability of the material is a feature that depends on the molecule chains. With the extension of the molecular chains, increase in molecular weight, the flow of the material becomes difficult and its viscosity increases. MFR testing is widely used in the evaluation of SLS powder [11,18,24,25].

The Gel Permeation Chromatography (GPC) method was used to analyze SLS powder at the macro molecular level[17,26]. In GPC method, the polymer material is dissolved in a solvent and separated according to the size of the molecule chains. Precise molecular weight, macromolecular properties and branching information of the polymer can be obtained. Wudy and Drummer[17] discovered that the molecular weight of the polymer exposed to high temperature for a long time is due to the linear chain growth mechanism as a result of their GPC test.

Calculating the surface tension of molten polymers is challenging, especially for polyamides. Compared with zero-shear viscosity, surface tension is a very weak function of the polymer type and the exposed temperature. Citing this reason, [26–28] dealt with changes in zero-shear-viscosity. Polymer materials are generally shear-thinning materials with a viscosity falling above a certain shear-rate. However, no shear force is applied in the selective laser sintering process, so low shear rates have been of interest, i.e. zero-shear-viscosity. Verbelen et al.[27] concluded that, zero-shear viscosity is a useful rheological property to evaluate the long-term usage, or aging, of polyamide powder.

DSC is a thermal analysis method [18] that helps to understand the behavior of polymers when they are heated. The melting characteristics of semi-crystalline polymers are often used to study the crystallization mechanism[29,30]. Using DSC thermograms (Figure 17); glass transition temperature, melting points and crystallization points can be obtained. Enthalpy of fusion (ΔH_f) and crystallization (ΔH_c) values can be obtained by integrating the heat flow area under the melting (T_m) and crystallization (T_c) peaks (Figure 17). By evaluating the enthalpy values, the crystallinity percentage(χ) of the semi-crystalline material can be calculated with the following formula[29];

$$\chi = \left(\frac{|\Delta H|}{\Delta H_0}\right) x\, 100 \qquad \text{(Equation 4)}$$

In this equation, ΔH_0 is the pure crystalline PA12 melting enthalpy (209 J / g), and ΔH is the melting enthalpy of the tested material.

Crystallization onset temperature can be postponed significantly by an increase in exposed temperature. Postcondensation reactions enhance by increasing temperature, this is why crystallization onset temperature decreases. As a result, molecular weight and melt viscosity increases. Therefore, crystallization kinetics become slower[27]. The sharpness of the crystallization peak can give information about the crystallization kinetics. A large peak refers to progressive crystallization.

During the melting of polyamide materials, it may be possible that not all crystals in the material can melt. This condition is called self-seeding, and its main reason is that some hydrogen bonds remain constant during melting. When self-seeding occurs, crystal regions that have not fully melted can form effective nucleation sites during cooling. The gradual increase of the crystallization onset value as a result of the DSC test on the material indicates that it may be self-seeding. If this happens during laser sintering, it is necessary to ensure that the material is fully melted by applying sufficient energy of laser energy to prevent self-seeding. By ensuring complete melting, the nuclei in the material disappear and thus premature crystallization is prevented [27].

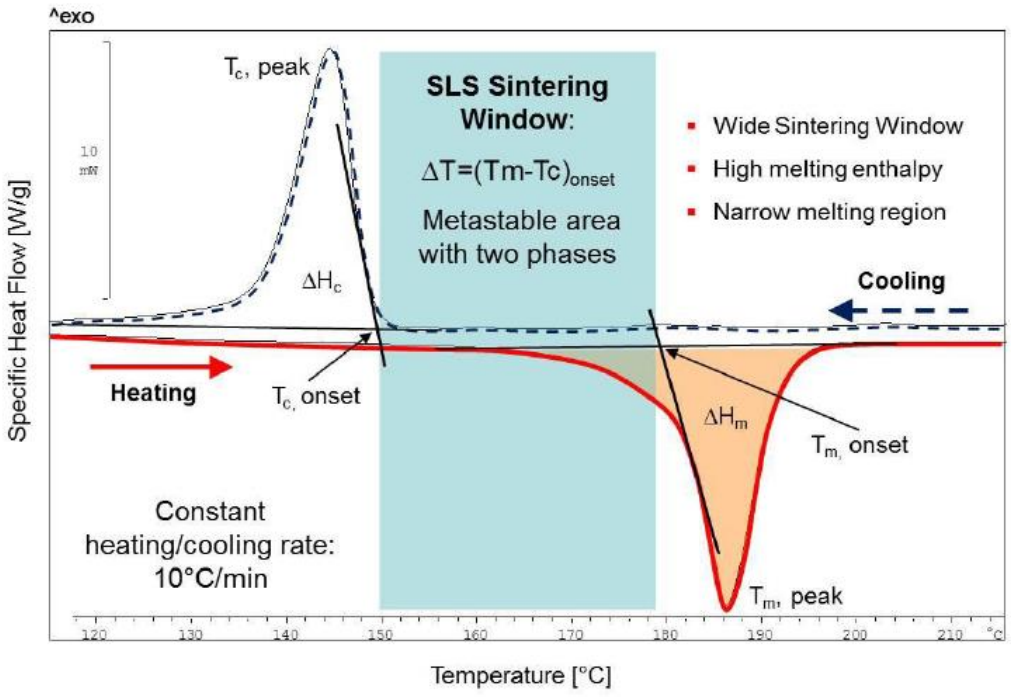

Figure 17 Demonstration of the sintering window on DSC thermogram [31]

The melting peak in the DSC plot gives important information about the laser sinterability of the material. A sharp and high melting peak is indicative of high melting enthalpy. Melting enthalpy also increases with increasing crystal perfection in the material. Since virgin powder has the highest crystallinity of the powder, its' melting peak is also the sharpest and highest. High crystallinity is very important for laser sinterability. During laser scanning of materials with high enthalpy of fusion, melting adjacent scanning region powders does not occur. At the same time, high-crystalline powders will have less aggregates when they stay in the temperatures above the glass transition temperature for a long time. Moreover, a steep melting onset and a narrow melting peak allow the powder to be used at higher preheating temperatures during the process. In this way, a better melting occurs with the scanning of the laser [27].

CHAPTER 3 DEVELOPMENT OF INNOVATIVE THERMAL MONITORING SYSTEM

3.1. Introduction

In the SLS process, temperature measurement and control is critical to ensure that there is no distortion and sufficient bonding between layers[1]. Therefore, temperature control in every region and every layer of production is also important. Thermal imaging is frequently preferred in the literature in order to measure this temperature story temporally and spatially. Information on some thermal camera systems installed to provide thermal imaging for SLS / SLM machines is shared in Table 1.

Table 1 Overview of the thermal monitoring systems used in selective laser sintering/melting process

Authors	Spectral Range	Resolution (pixel)	Frame Rate (FPS)	Window	Camera Position
Yuan and Bourell [32]	LWIR	320x240	60	ZnSe	In front of the viewing window
Diller et al. [33]	LWIR	320x240	60	ZnSe	In front of the viewing window
Krauss et al. [34]	LWIR	640x480	50	Germanium	In front of the viewing window
Fish et al. [1]	LWIR	320x240	60	ZnSe	Adjacent to scanner head
Wegner and Witt [16]	MWIR	320x240	60	ZnSe	Adjacent to scanner head
Abdelrahman and Starr[35]	MWIR	640x512	100	ZnSe	In front of the viewing window

The systems installed in front of the viewing window of the machine were prepared by changing the front window of the machine and placing a camera in front of it. Due to the low viewing angle in these systems, measurements can be made incorrectly due to high reflection and low emissivity in these angles. At the same time, the view of the parts is not effective. The most effective view is provided by the method obtained by placing the camera adjacent to the scanner head, but for this, the sheet metal of the build chamber must be cut. Zinc Selenide windows were used in most of the works.

3.2. Materials & Equipment

The thermal monitoring kit consists of four different parts. These parts are; LWIR camera, camera housing, data transfer cable and cooling system.

The housing of the camera was produced by SLS process, using glass-bead and aluminum-stamp filled PA12 powder. High temperature resistant silicone gasket was used at the joints of the parts to make the casing airtight. Glass wool was used to provide wall insulation of the enclosure.

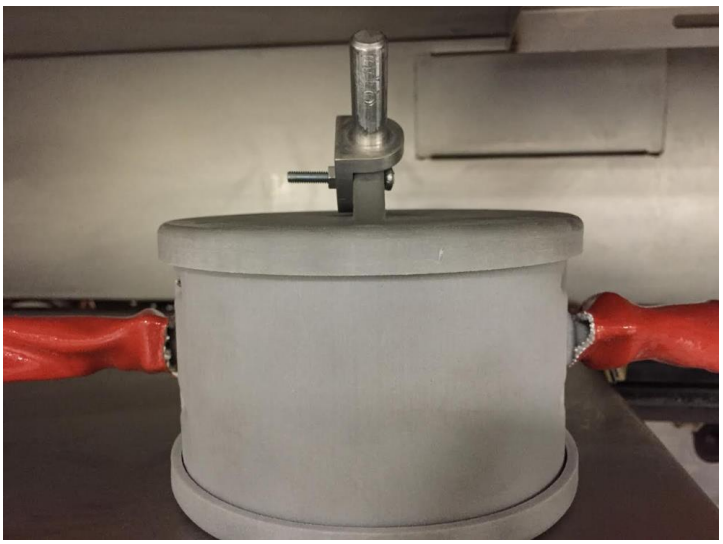

Figure 18 Thermal camera housing with silicone pipes connected on both sides

In the housing viewport, an AR (Anti-Reflective) coated ZnSe (Zinc Selenide) window is used. AR-Coated ZnSe window (Figure 19) preferred due to its transmittance, reflectance and emittance. These factors affects the level of radiation reaches through the window[36]. This window provides over 90% transmittance for LWIR (8-14 μm).

Figure 19 AR-Coated ZnSe Windows

The DTM Sinterstation 2500 Plus has a nitrogen generator connected to it so that it can provide the appropriate nitrogen atmosphere during production, and this nitrogen generator has an air compressor to produce nitrogen. Cooling of the housing is provided by the stable 19C air coming from this compressor. The transfer of air from the compressor line to the casing and discharge from the casing out of the machine is done with silicone pipes. These pipes were used by inserting them into silicone coated glass fiber sleeves to provide insulation.

Optris Compact CT pyrometer (Figure 20) was used to verify the measurements made with the thermal camera. It's emissivity has adjusted to 0.98[17] for the measurements.

Figure 20 Optris Compact CT pyrometer

A high temperature resistant USB 2.0 cable has been produced for data transfer from the LWIR camera to the computer. Fluoropolymer coated wires in 28AWG standard for data

transfer and 24 AWG standard for power transfer and grounding are used. These wires can withstand temperatures up to 205C. Silicone tape is used for the structural insulation of the wires and aluminum foil is used for the signal insulation. Finally, the silicone coated glass fiber is wrapped in tubing.

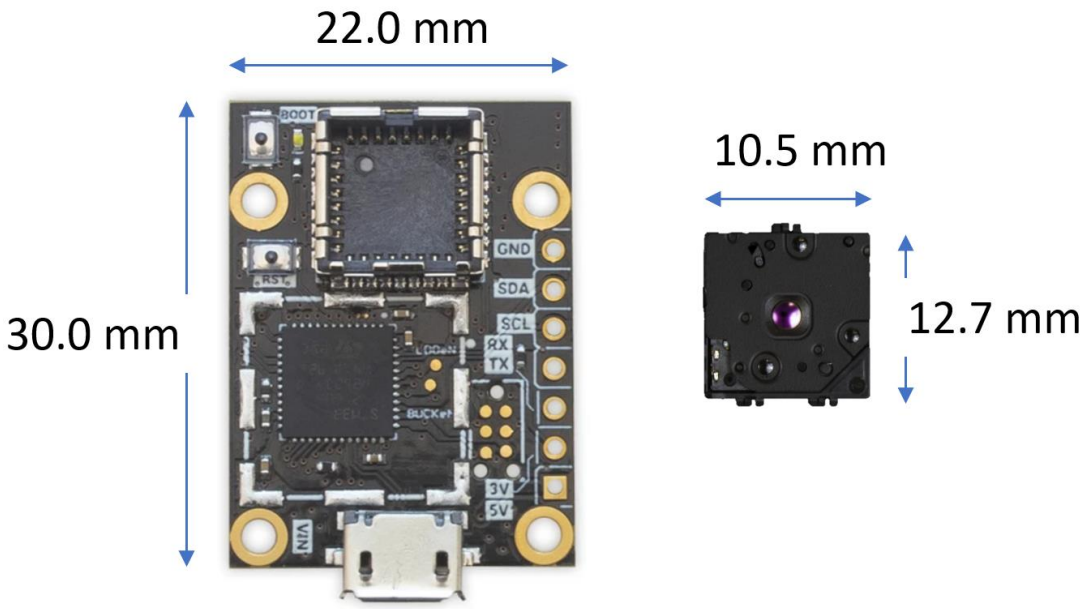

Figure 21 PureThermal 2 interface electronic board (left), Lepton 3.5 Radiometric LWIR Module (right)

FLIR Lepton 3.5 module (Figure 21, right) with uncooled microbolometer detector was used for thermal imaging. The thermal module has a resolution of 160 (horizontal)×120 (vertical) pixels, and a reported accuracy of ± 5 °C, frame rate of 9 Hz, and a spectral response wavelength range of LWIR (8–14 μm). The horizontal field of view (HFOV) of the module is 57°. A PureThermal 2 breakout board (Figure 21, left) with the SPI communication method was used to acquire data from the module.

3.3. Innovative Thermal Monitoring System

In this study it was aimed to develop a thermal monitoring system without permanently modifying the Sinterstation 2500 Plus machine. Previous studies[12,16,32–35] installed thermal monitoring systems by modifying the SLS machine whether removing the front window of the machine or cutting a place for the IR camera beside the scanner unit. There is no way to install the thermal monitoring system from outside of the SLS machine

without modifying it. Therefore, it is decided to place the camera inside the build chamber from attaching it to the screws of laser window holding unit (Figure 23).

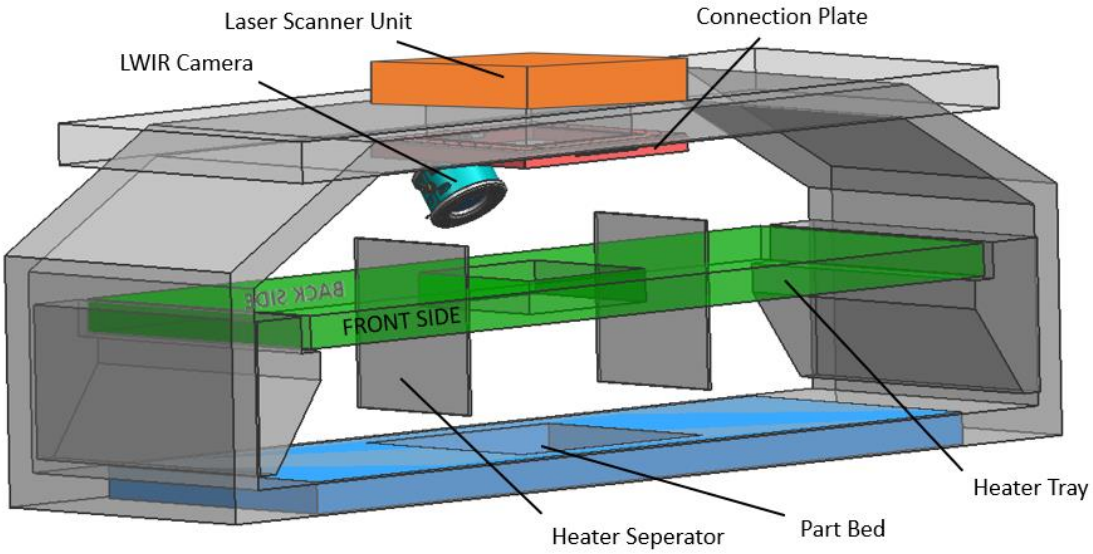

Figure 22 Thermal monitoring system installed on Sinterstation 2500 Plus

Preliminary examination is done before designing the thermal monitoring system. The most precedence constraint is the temperature inside the build chamber. Since the Lepton 3.5 LWIR camera has the maximum operating limit of 80°C, it is required to work below this temperature. Therefore, thermocouples placed inside the build chamber to measure; ambient temperature and chamber surface temperature. While there is an ongoing build on the machine, the highest ambient temperature and the highest surface temperature measured 110°C and 150°C respectively. Consequently, it is needed to protect the LWIR camera by covering it to prevent from high temperatures. In view of the fact that PA12 material has endurance to temperatures that measured in the chamber, the protective housing manufactured from PA12 material by SLS process. The design of the housing revised few times before it completed. Owing to additive manufacturing technology, without tooling and a mold, which makes it possible to obtain the product within the day after the design is completed.

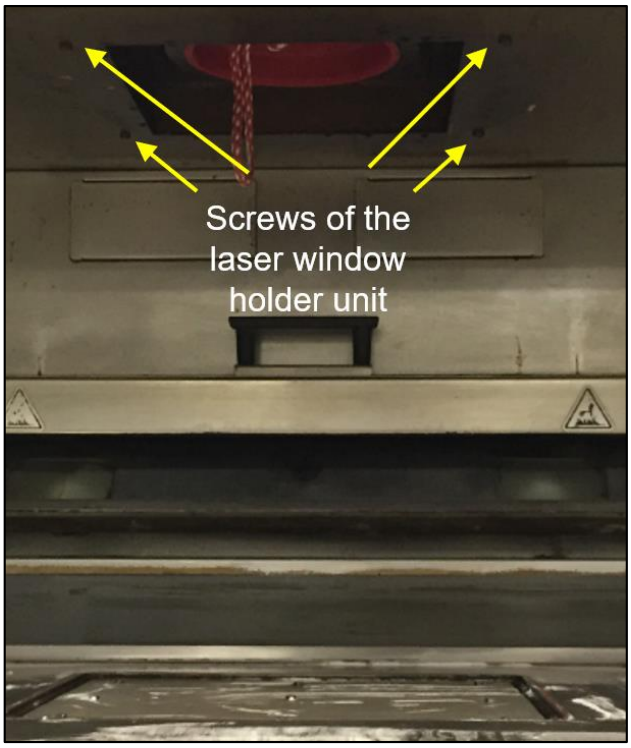

Figure 23 The place where the connection plate installed

It is important to determine the heat transfer mechanisms inside the chamber to design the protective housing. Sinterstation 2500 Plus heaters, heats up the powder bed by radiation. In order to inert the build chamber, nitrogen gas blows into chamber from the nitrogen generator. This nitrogen flow in the chamber leads to convective heat transfer from hot surfaces. Since the protective housing is mounted to chamber by connecting link, there is conductive heat transfer towards the housing. For the purpose of decelerating the heat transfer by conduction and convection, top and lateral walls of the housing filled with glass wool. Fish et al.[1] used double layer of ZnSe window for their LAMPS(Laser Additive Manufacturing Pilot System) laser entrance window. However, using second window is additional cost and volume increasing factor for the housing. Using a uncooled ZnSe window is unsatisfactory for absolute measurements because it will effect absorption coefficient and IR transmission of the window [37]. Since therefore, a flap designed and placed in front of the air intake for cooling down the window much better. By adding a flap, the temperature of the window decreased to 65°C from 92°C.

The advantageous sides of the protective housing are it is much cheaper than stainless steel housings in the market and it can be producible by the SLS machine for itself. Air cooling system used for expelling the hot air from the housing. The stability of the thermal camera sensors is of great importance in terms of accurate measurement. Stable 39°C

sensor temperature is provided by air cooling connected to the housing. This cooling system connected to air compressor of the nitrogen generator of the Sinterstation 2500 Plus.

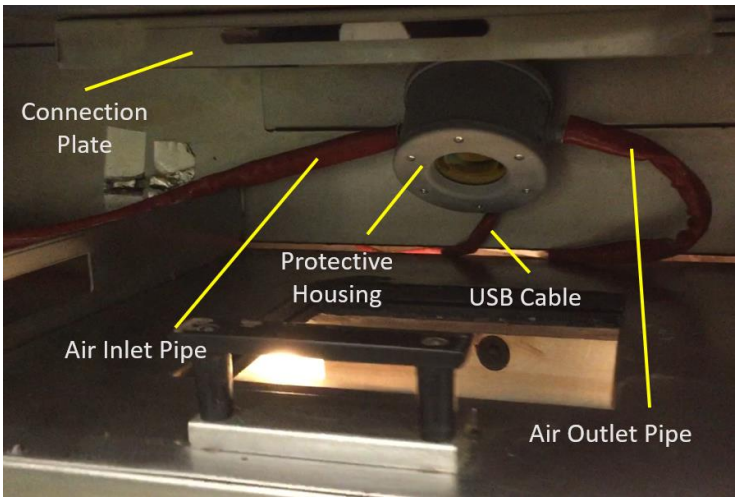

Figure 24 Protective housing inside the build chamber

The connection plate mounted (Figure 24) to build chamber of Sinterstation 2500 Plus. It can be easily removed from the chamber without giving any damage to machine. While recording an image or a video the recording device, LWIR camera, must be as rigid as possible to prevent aberrations due to the vibrations. Therefore, all junctions tightened greatly. Since the Sinterstation 2500 Plus is a stationary machine, no vibration damping element has used.

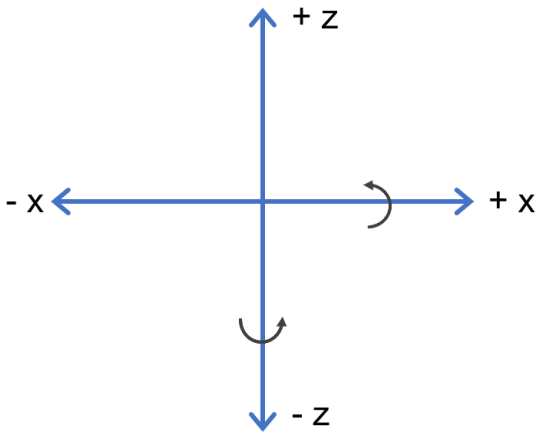

Figure 25 Translation and rotation criteria for the protective housing

This thermal monitoring is system designed to adjust the point of view as intended, while ensuring the robustness. To achieve the freedom of motion, translation and rotation criteria is designated as shown in Figure 25. According to these criteria, the LWIR camera can be translated and rotated both on x and z axis bidirectional. The plate has a channel on itself to able moving two-sided on x-axis. All rest of the motions; x-axis rotation, z-axis rotation and z-axis translation are provided by the connector link between the housing and the plate. In Figure 27, motion capabilities of the protective housing shown. There is an angle of 35° between the viewport and the build plate, illustrated in Figure 26.

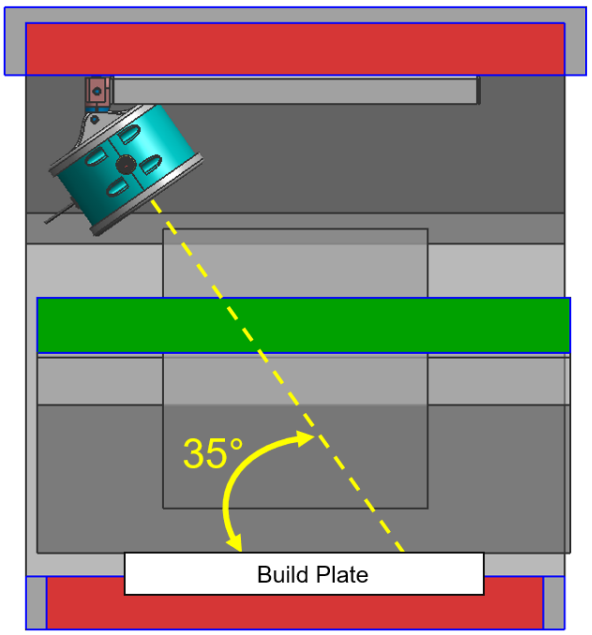

Figure 26 Viewport angle of the LWIR camera

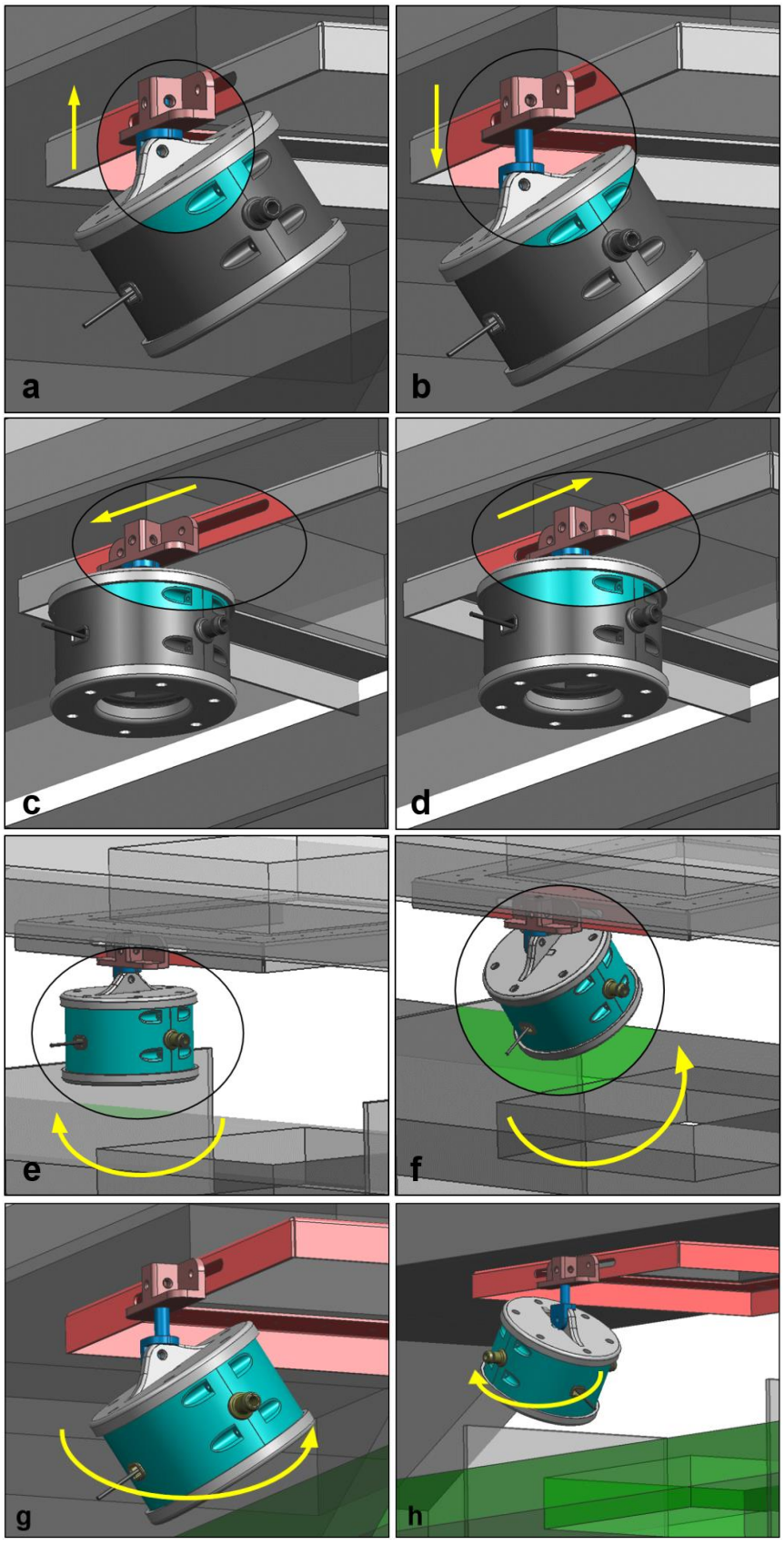

Figure 27 Axes of movement for the protective housing. Translation on z-axis (a-b), translation on y-axis (c-d), rotation on y-axis (e-f), rotation around z-axis (g-h)

CHAPTER 4. THE EXPERIMENTAL DESIGN & INVESTIGATION OF THERMOGRAPHIC MEASUREMENTS

4.1. Introduction

Thanks to process monitoring systems; It is used in applications such as quality reporting, providing feedback control and error detection[34,35]. In this way, the sustainable quality of the part can be verified, process parameters and the process can be improved. Fish et al.[3] developed an adaptive laser control system by evaluating the data obtained by thermal imaging. They managed to ensure that the laser power is adjusted according to the temperature of the regions.

Abdelrahman and Starr[2] indexed the temperature data obtained in thermal imaging to the 3D data of the part. They have developed a 3D quality verification method that will mark the regions where the temperature is below a certain value as defective on the 3D temperature image obtained. In another study[35], they observed that the temperature of the layer changes depending on the cross-sectional area of the part and developed a feed forward control system to reduce the temperature difference between layers.

Wegner and Witt[16] inspected the performance of their SLS machine by measuring the temperature distribution in the part bed heaters and the part bed with thermal imaging. Then, in the recording they made during production, they examined the effect of different process parameters on process temperatures.

Wroe[4], drew attention to the uneven temperature distribution in the part bed. He showed that the mechanical properties of the parts produced in different regions change due to the uneven temperature distribution.

4.2. Exploring the Innovative Thermal Monitoring System

After completing the protective housing of the LWIR camera, the thermal monitoring system installed to Sinterstation 2500 Plus. In the first exploration build, it was aimed to explore the required conditions for the experimental study. These are; minimum detectable object, the point of view and the heat distribution on the powder bed. For the test build, the designed specimens were pair of a square rod and a box. The square rod located in the box with a definite distance between the wall and a definite wall thickness. There were eleven pair of specimen; seven of them have boxes with same wall thickness of 3 mm, ID# specimen, and particular inter-part distances (#: 1, 2, 3, 4, 5, 6, 7 mm) between box and the rod; for the last four pair, WT# specimen, all they have same inter-part distance of 4 mm but each have different wall thicknesses (#: 1, 3, 5, 7 mm).

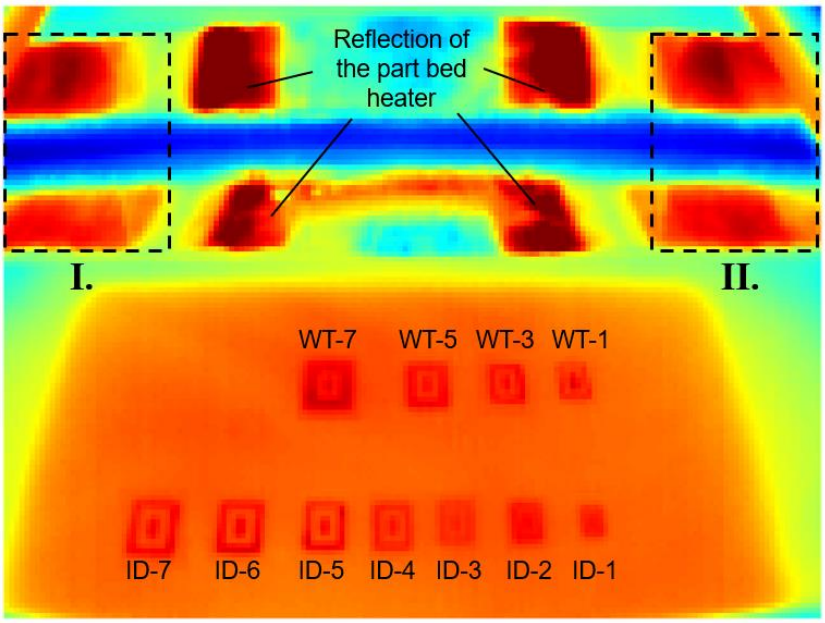

Figure 28 An image from the exploration record

In Figure 28, thermal image from the exploration video is shown. Region I. and II. Are reflection of the right and left feed heater respectively. Upper side of these regions are sheet metal of the Sinterstation 2500 Plus's front door, below side is the place where the powder ending on the powder bed.

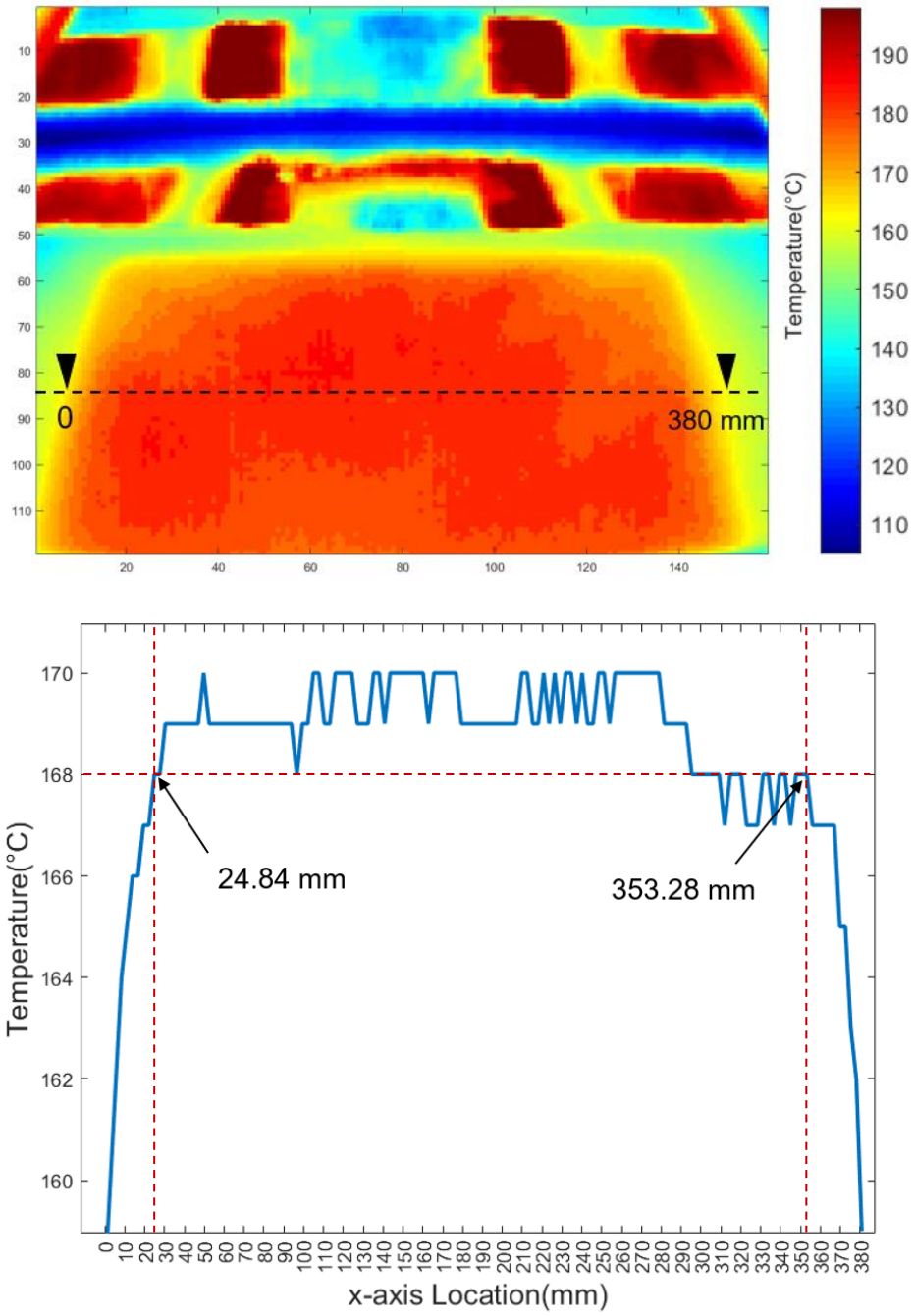

Figure 29 Thermography from the IR camera (above), temperature gradient of the specified section on the x-axis

Resulting from the view angle, the part bed is like a trapezoid and it becomes narrower when look at the further side. Since then, the absolute size of a pixel is changing from 2.55 to 3.25 mm. In other respects, within the ID specimens it had seen that the powder between the rod and the box is distinguishable, starting from the specimen ID-3. According to these inferences, the minimum inter-part distance decided as 3mm for the experimental study. When examining WT specimens, due to the absolute size of a pixel,

1mm wall thickness is not inspected. For the WT specimens, the region of interest (ROI) selected as each pair of specimens. Then, average temperature of each ROI taken and analyzed in MATLAB. The results showed that the average temperatures of WT-3, WT-5 and WT-7 are 170.1°C, 172.1°C, and 173.4°C respectively. There is not a noticeable difference found between WT-5 and WT-7, around 1°C. Thus, the wall thickness of WT-3 and WT-7 specimens decided for the experimental study.

Thermography of the process is given in Figure 29; part bed can be seen in different colors. Wegner and Witt[16] mentioned about the inhomogeneous temperature distribution on the part bed. The temperature distribution on the part bed is given for the 85th pixel row. There is 12°C temperature difference measured on the dashed line. Part bed temperature was set at 169°C on the build software. If the part bed set temperature considered as the boundaries for homogeneous temperature distribution there will be very limited build area on the part bed. Thus, 168°C decided as the boundary limit for the part bed temperature. To provide this requirement, there should be minimum 27.72 mm and 24.84 mm margin for the left and the right sides, respectively.

4.3. Experimental Design

In this study it was aimed to analyze both part and the powder under specified conditions, different wall thicknesses of the adjacent part and different inter-part distances. Thanks to AM, it is possible to prepare powder specimens by trapping it in a box [25].

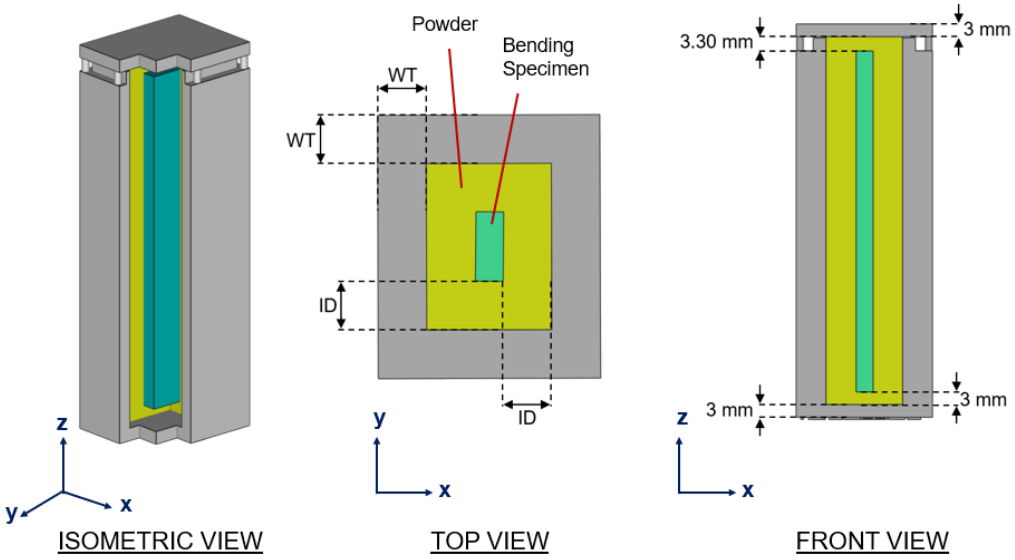

Figure 30 Geometrical constraints of the specimen pair

The samples used for this study is a pair of parts. The three-point bending specimen is placed in a box for the experimental studies. According to EN ISO 178[38], preferred dimensions for the three-point bending specimen has used; 4 mm x 10 mm x 80 mm. The box specimen has used for two reasons; acting as an adjacent part for the bending specimen and carrying the powder inside without messing it up. An easily breakable cover, shown in Figure 31, designed for opening the box easily for specimen preparation. The cover is surrounded with tiny connecting columns with a diameter of 1.8 mm and there is 0.3 mm gap has left intentionally for opening it handily, it can be seen from Figure 31.b.

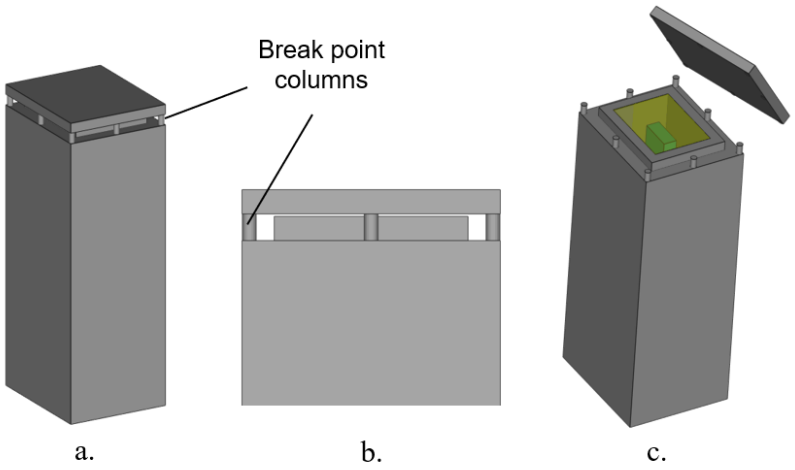

Figure 31 Demonstration for opening the cover. a) Isometric view of the sample b) Side-view of the sample focused on cover c) Sample with the opened cover

WT and ID parameters used in the design of the sample pair are shown in Figure 30. The chosen parameters are only changing in x and y axes, shown at top view in Figure 30. For all sample pairs, distance to the top and the bottom of the box are 3.3 mm and 3 mm respectively. Also, the top and bottom thickness of the box is constant, 3mm, for all sample pairs. The names and the parameter values of the samples are shown in Table 2. There is an additional sample just named as "BOX". This sample is designed to examine the change in powder after a one build, regardless of the parts. The wall thickness of the BOX is 1.5 mm and the distance between the inner walls of this sample are 22 mm and 37 mm.

Table 2 Sample parameters for the experiment

Sample	Inter-part Distance (ID)	Wall Thickness (WT)
ID7-WT7	7 mm	7 mm
ID7-WT3	7 mm	3 mm
ID3-WT7	3 mm	7 mm
ID3-WT3	3 mm	3 mm

For the analysis, it was planned to produce four of each sample pair. The build packet was prepared as in the Figure 32 considering the margin values determined in Chapter 3.2. The "Blind Zone" is the area outside the field of view and covers approximately 27% of the build area. Which equals to 73% of the build platform is visible. The reference area, where the pyrometer measures, is shaded in red. In order to verify the measurement values made with the thermal camera, it was planned to measure throughout the production with a calibrated pyrometer of the reference area.

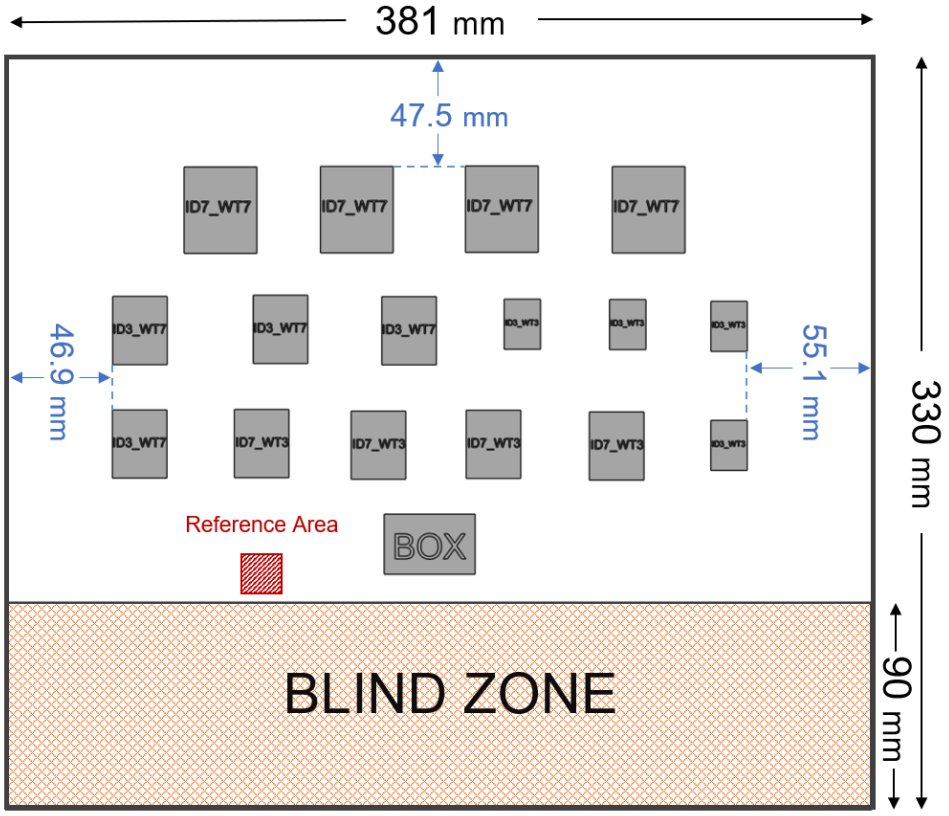

Figure 32 Detailed 2D-view of the build

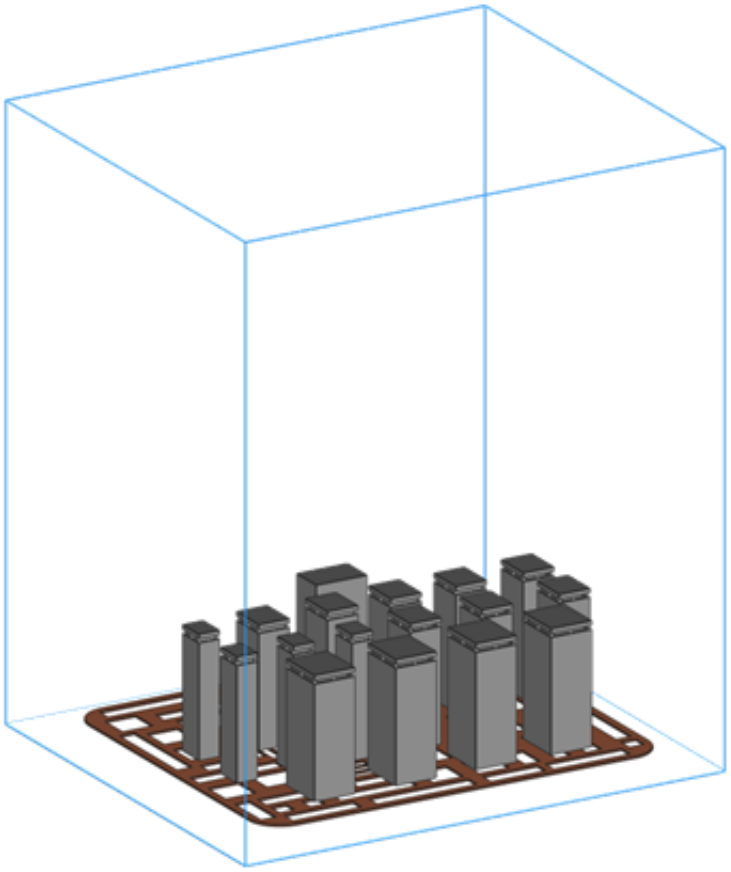

Figure 33 Isometric view of the build packet on Materialise Magics software

4.4. Investigation and Interpretation of Thermographic Measurements

IR Thermography video recorded from the FLIR Lepton User App software. The recorded raw data was TIFF file format. In each recorded TIFF file, there are thousands of thermal image frame and each frame has 160x120 pixels resolution. The temperature data belonging to each pixel is also stored in the pixels of each frame. For the video record, the frame rate of 8.7 fps used, which is default for Lepton 3.5 LWIR camera. The calculations of thermographic measurements are processed by MATLAB. For the experimental study, 14.5 hour of build completed in Sinterstation 2500 Plus and video is recorded by the LWIR camera. Saved thermal video size is about 21 GB. There are 461,002 frame exists in the TIFF file of the total recording.

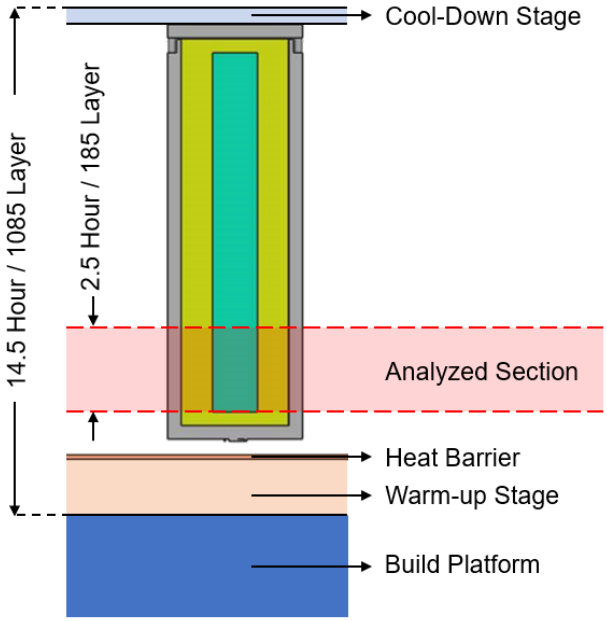

Figure 34 Section view of the specimen on the build platform

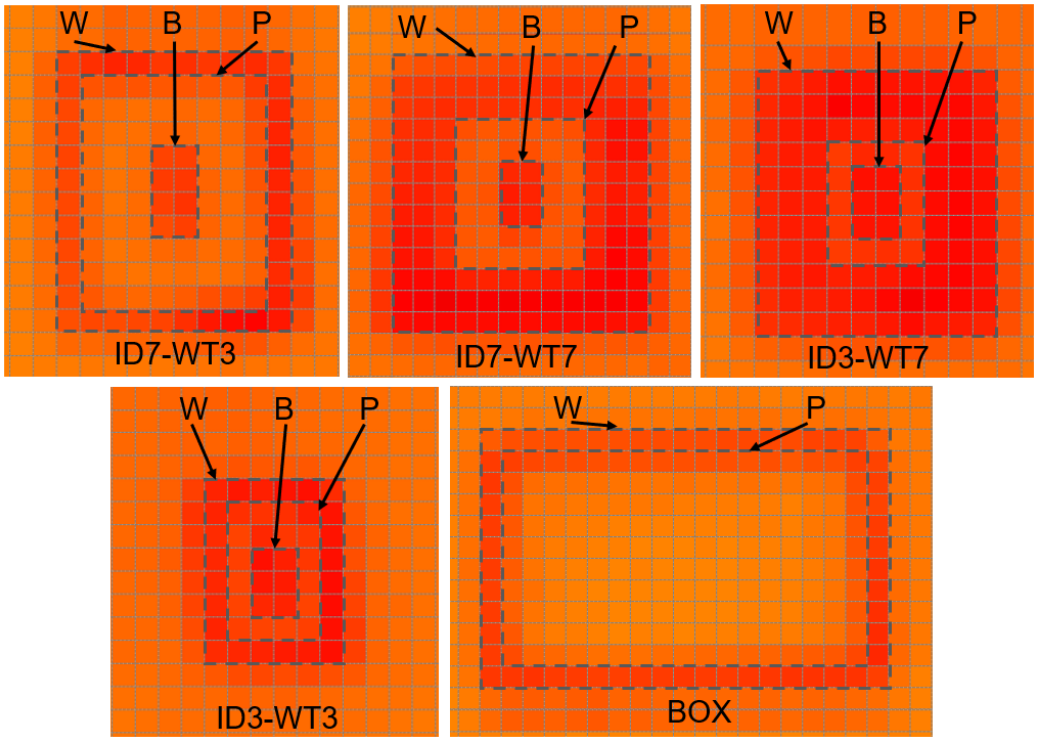

Figure 35 Region of Interest (ROI)'s of each specimen pair is shown

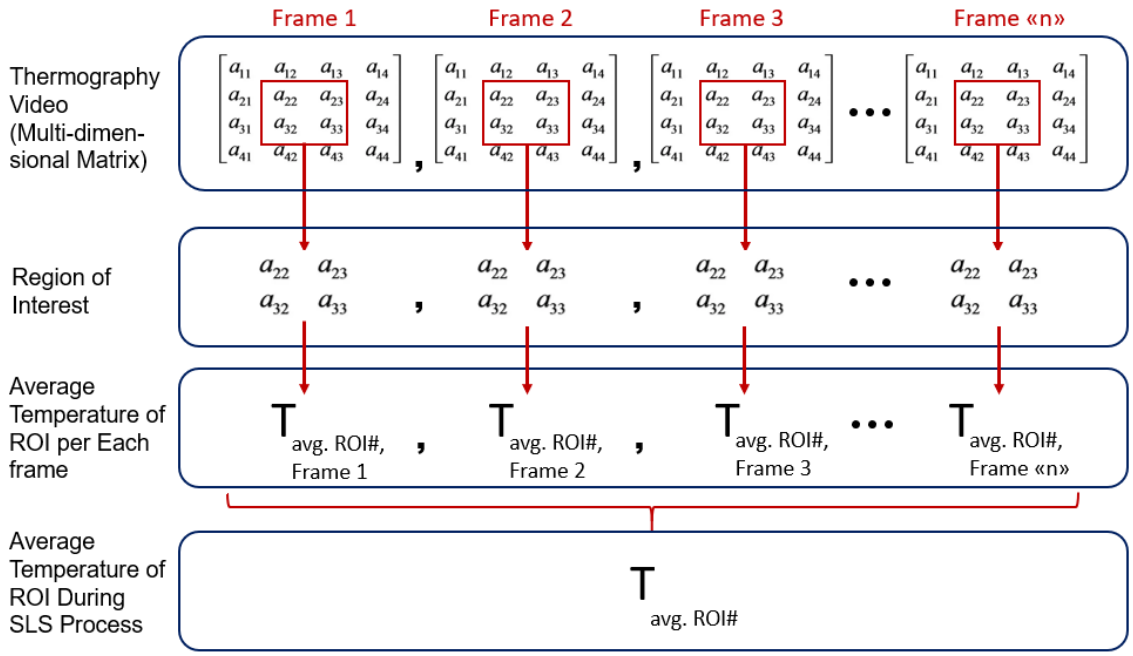

Figure 36 Representation of the ROI temperature calculation method

The TIFF file can be considered as three-dimensional matrix. First two dimension stands for the x (160 columns) and y (120 rows) axis of the frame, the third one represents the frame number.

In the first step of the temperature analysis, the regions of interest (ROI) were determined in each sample of interest (Figure 35). From these regions; "W" represents the wall thickness of the adjacent part, "P" represents the powder between the bending sample and the adjacent part, and "B" represents the bending sample. Since there is no bending sample in the BOX sample, only the outer wall and the internal powder temperatures were examined in this sample. The determined ROIs were processed in MATLAB using the method shown in Figure 36. In this method, after determining the ROIs, the average temperature value of the specified ROI is calculated for each thermography frame, which represents the value of the ROI in that frame. Then, the values of each square are averaged for the relevant ROI. This result value represents the average temperature value of the selected ROI.

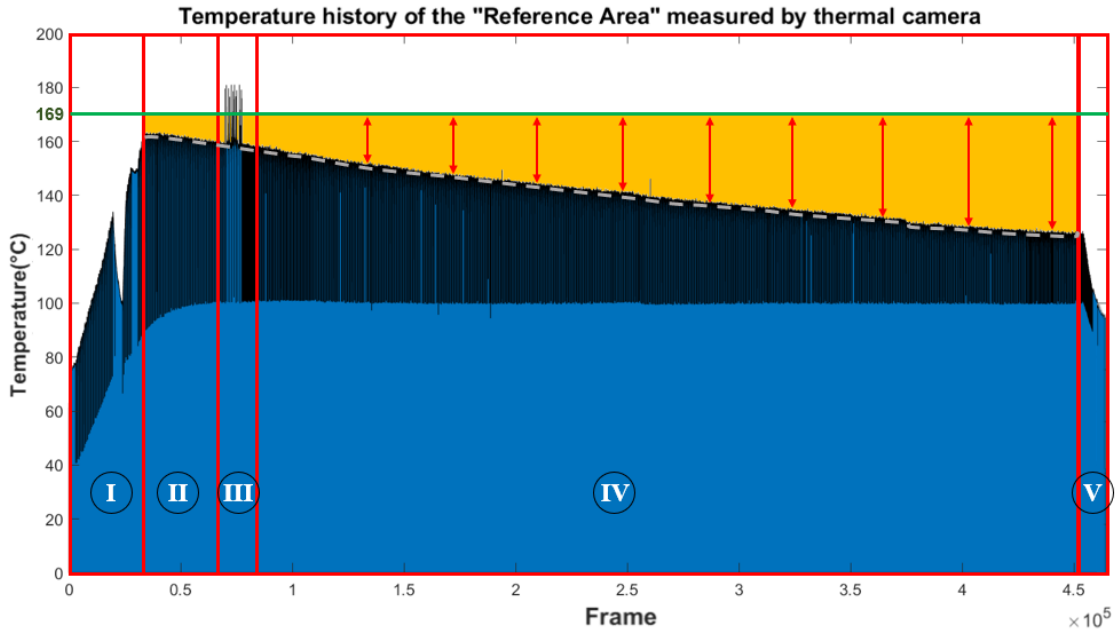

Figure 37 Temperature history of the "Reference Area" measured by thermal camera

It was observed at the 14.5 hours of long run production, reference area temperature measured by the IR camera (Figure 32) decreased continuously with the rate of approximately 3(°C/hour). However, there is no similar drift at the pyrometer measurement results. The value measured by the pyrometer is the input signal of closed-loop powder bed heater control system[4]. If there is any kind of error/drift at the pyrometer measurements, SLS process will be affected by this temperature issue. Besides, there is not any failure occurred during the process. Since therefore, pyrometer measurements assumed as the absolute temperatures. The temperature value of the reference area shown in Figure 37 was measured by both the thermal imager and pyrometer, and the temperature difference between the two values was calculated for each frame. This value difference was compensated in each relevant frame by adding it to the measured value of the relevant ROI analyzed by the thermal imager.

In Figure 37, green line at 169 °C presents the value measured by the pyrometer for the reference area. The divergence from the absolute temperature value can be seen at the orange colored area. There are 5 different section shown;

I. This section is the warm-up stage. The temperature of the powder increases continuously until reaching at the target temperature (169 °C).

II. When the target temperature has achieved, the warm-up stage ends and process continues to hold the powder bed temperature at a stable regime.

III. These peaks show that laser scanning occurred. In the early stages of build, the build platform is colder and a heat barrier is built to prevent its effect on parts. The peaks belong to the scanning pattern of the heat barrier. In Figure 34 the location of the heat barrier can be seen clearly.

IV. The fourth section is the building stage. Since there is no part located in the reference region, a peak was not observed after the heat barrier.

V. The last phase of production, that is, cool-down stage. The part bed temperature is gradually decreasing.

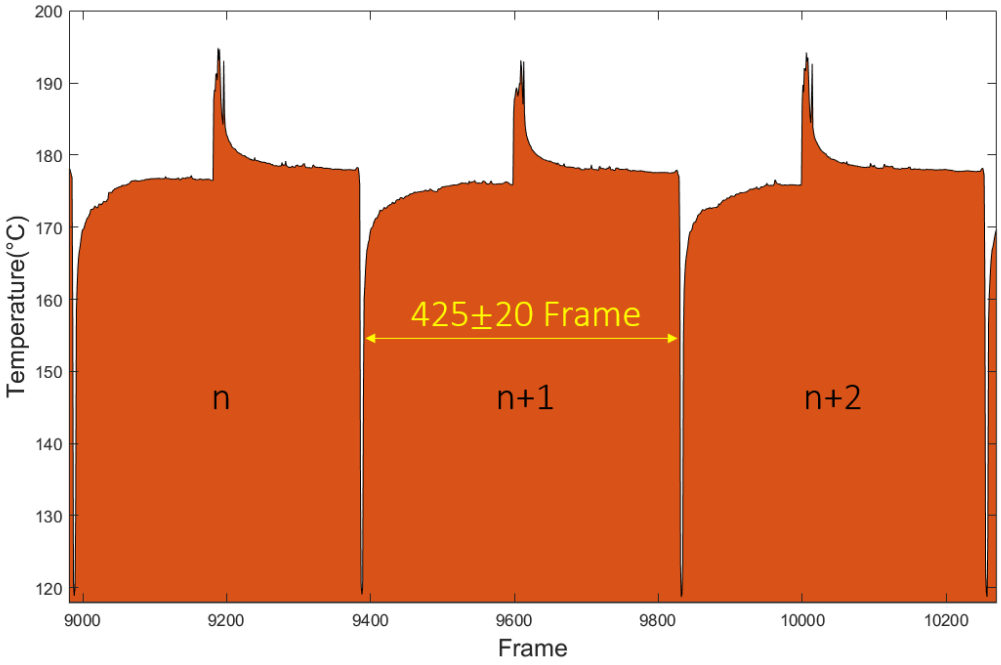

Figure 38 Labeling of the layers on Temperature-Frame graph

In Figure 38, n, n + 1 and n + 2 indicate successive layers, respectively. In the experimental production, each layer consists of 425 ± 20 square images. If the frame rate of the LWIR camera is calculated as 9 Hz, the production time of each layer is approximately 47 ± 2 seconds. When we get closer to the graphic, we see two valleys. The instantaneous temperature drops here indicate the moment the spreader passes from the point where the measurement is made. The region where the process in the layer continues, that is, between the two valleys, where the temperature suddenly rises, indicates the laser sintering of the monitored area.

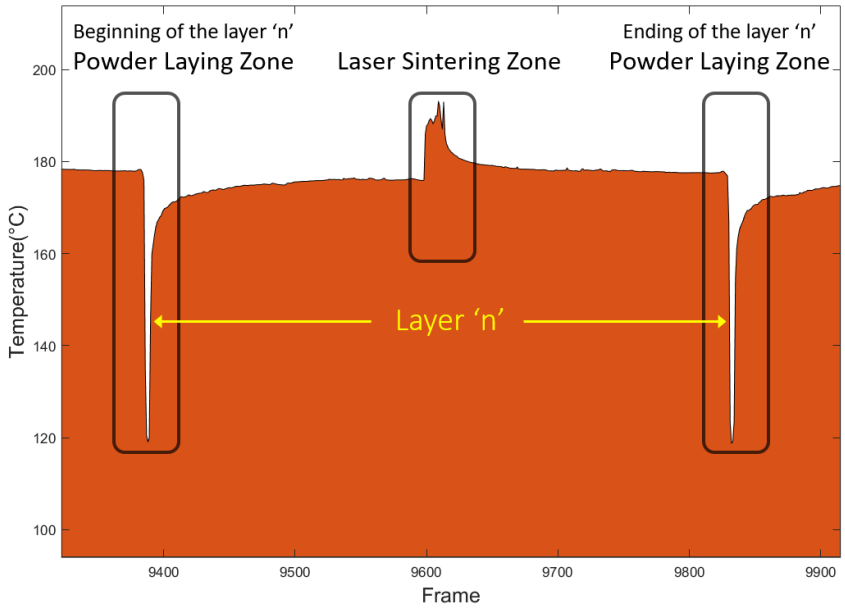

Figure 39 Interpretation of the graph for a single layer

In the Figure 39, the area where the laser is sintered is enlarged. We realize that the single peak seen from a distance actually consists of more than one peak. It is seen that there are especially two separate regions. Here, the region "1" indicates laser scanning of the infill, and the region "2" indicates the laser scanning of the outer wall. Since the outer wall scan is only along a single line of scan, it is faster than the inner fill, and therefore the width of "1" is more than "2". Since the laser scanning power of the outer wall is lower than that of the inner filling, the height of "2" is less than "1".

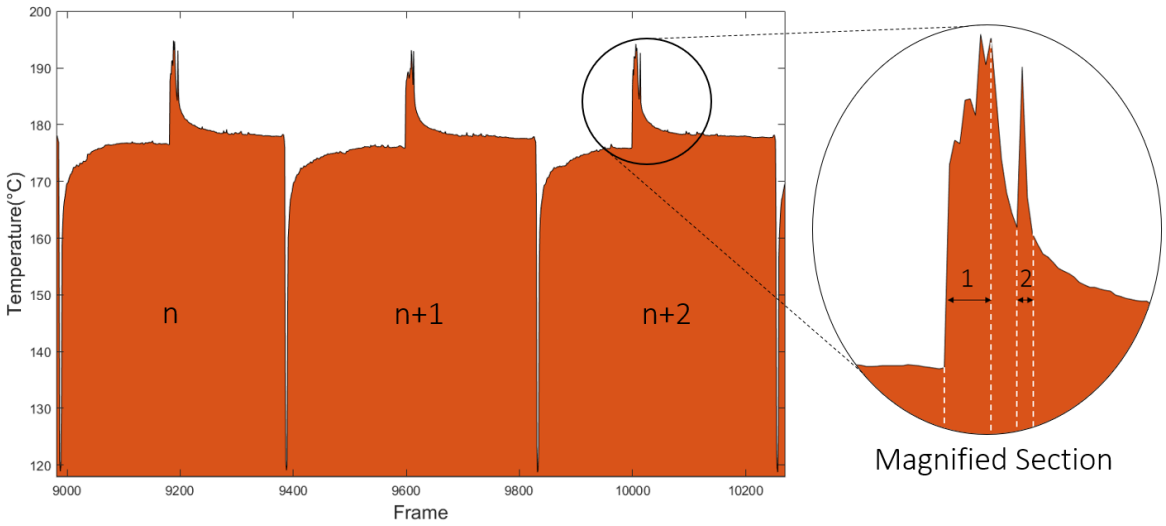

Figure 40 Detailed demonstration of the sintering zone

At the end of the process, window of the protective housing was contaminated, which is omnipresent issue in industry[39]. Previous studies mentioned that the high build

chamber temperatures and laser sintering of polymer, outgasses chemical by-products. Water vapor is one of these gases[39–41]. Sassaman et al.[39] presented that the distribution of the contamination is not uniform across the ZnSe window and unrepeatable amongst each build. Since the laser beam scans through laser window within 2D area, information about single point contamination is not enough to analyze effects on the process. They constructed a low-cost photodiode power meter to measure laser power attenuation at the ZnSe window on 2D area and suggested that intra-layer laser power attenuation deviates around 3.5%±0.25%. Further, they noted there is a correlation between the number of layers and window contamination. Reducing the window contamination practiced by two approaches; heating up window to hinder contamination[40] and purging inert gas towards the window to form gas curtain[41].

z 

Figure 41 Left, protective housing window before the process. Right, contaminated window after the process.

CHAPTER 5 INVESTIGATING THE EFFECTS OF NESTING DESIGN

5.1. Experimental Study

In the production stage of this study, 50% glass bead filled PA12 powder (PA 615 GS) material used from Advanced Laser Materials (ALM). Only virgin powder was used in the production of the parts. From the technical data sheet of the powder according to ASTM D3418 standard, the virgin PA 615-GS melts at 186 °C. However, only the bending module of the part produced in the XY plane was shared, which is 3,100 MPa according to the test performed in the ASTM D790 standard. All parts are built with the same parameters specified by the powder manufacturer.

For the data shared in the results section, the sample names are given as ID # -WT #. It refers to the distance between parts (ID) of the sample pair and the adjacent part's wall thickness (WT) parameters. In order to make the test results repeatable, four samples were produced from each sample.

5.2. Thermographic Analysis

The methodology described in Chapter 4.4 was used to evaluate the results of thermographic measurements. Temperature history distributions of ROI's starting from 160 °C to 195 °C are shown in Figure 42-44 with 5 °C intervals. Temperature distribution graphs were used to evaluate which temperature the sample was exposed to longer. Wudy and Drummer[17] have revealed that the aging time of powder has a more significant effect than the building temperature. For this reason, it will be critical to evaluate the distribution graph of the temperature values in Figure 42-44. Since the majority of the values are distributed in the range of 160-180 °C, the distribution over 180 °C cannot be interpreted by this graph. Thus, the mean of temperature values above 180 °C are shared

in Table 3 separately. In Figure 45, the average of the temperature values above 180 degrees is given and compared for each sample and ROI separately.

The effects of inter-part distance and wall thickness factors on the temperature of the powder, bending sample and the wall part were interpreted by examining the temperature distribution (Figure 42-44) and the average temperature above 180 °C graphs (Figure 45).

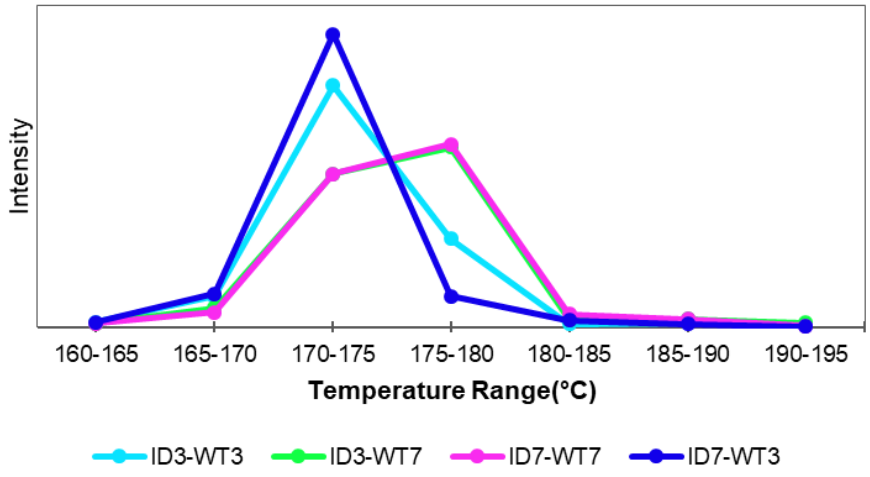

Figure 42 Distribution of the temperature for the wall parts of the samples

The temperature story of the wall part is examined, by increasing the wall thickness from 3 mm to 7 mm, the temperature concentrated distribution of the samples were increased from "170-175" to "175-180" range (Figure 42). When looking at their average above 180 °C (Figure 45), the effect of inter-part distance seems to be more prominent. Moreover, an increase at the temperature of the wall observed as the distance between the parts decreased from 7 mm to 3 mm.

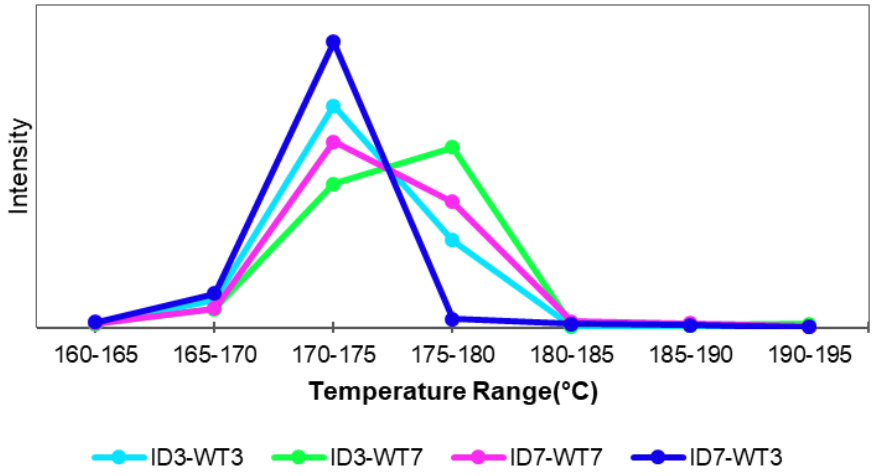

Figure 43 Distribution of the temperature for the powders of the samples

When the temperature story of the powder between the parts examined, it was observed that it showed the same impact as the wall piece. In the temperature story of the bending sample, the same effects were observed as in the other parts. But unlike others, the maximum difference between the bending parts of the samples in the average temperature above 180 °C is, 1.6 °C. However, this difference is 8.4 °C and 5.5 °C, respectively for the powder between the pieces and the adjacent wall. A value called "mean of sample" is shown in Table 3. This value represents the average of the bending part, the powder and the wall temperatures for each sample.

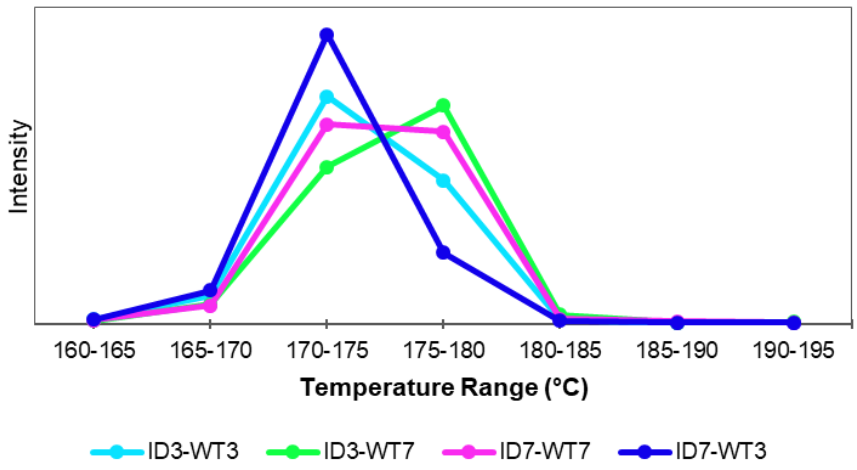

Figure 44 Distribution of the temperature for the bending parts of the samples

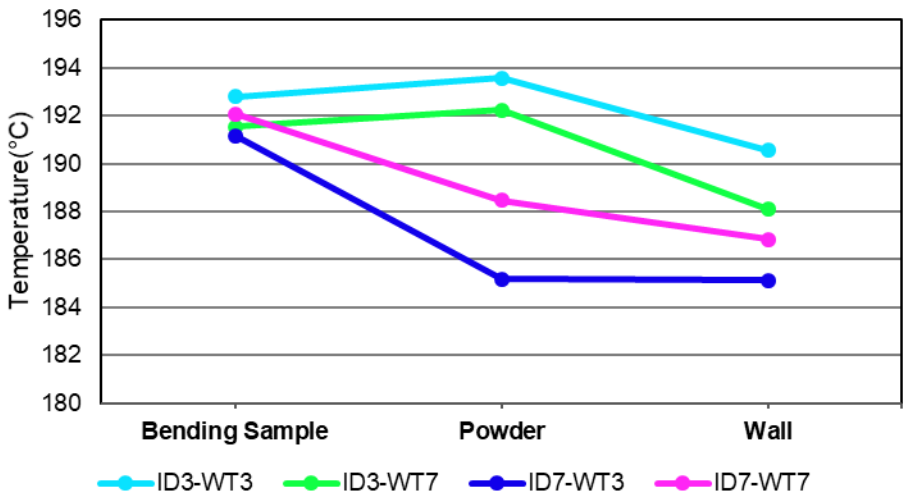

Figure 45 Temperature history of the parts (average of temperatures above 180°C)

Table 3 Average of the part temperatures above 180 °C

Sample	Bending Sample	Powder	Wall	Mean of Sample
ID3-WT3	192.8 °C	193.6 °C	190.6 °C	192.3 °C
ID3-WT7	191.5 °C	192.2 °C	188.1 °C	190.6 °C
ID7-WT7	192.1 °C	188.5 °C	186.8 °C	189.1 °C
ID7-WT3	191.2 °C	185.2 °C	185.1 °C	187.2 °C

5.3. Three Point Bending Analysis

Zwick Z020 Universal Testing Machine (UTM) was used for three-point bending tests. The test was carried out on samples of 4 mm x 10 mm x 80 mm in accordance with EN ISO 178 standard at 1mm / s speed. Four replicates were performed for each sample type.

Figure 46 Zwick Z020 Universal Testing Machine

The average results of four replicates for each sample are shared in Table 4. Figure 47-48 shows the effects of the temperature that the parts are exposed to during the manufacturing process on the flexural modulus (E_f) and flexural strength (σ_f). The temperature data used here are the values in the "Bending Sample" column in Table 3.

Table 4 Three-point bending test results

Sample	σ_f (MPa)	E_f (MPa)	e (%)
ID3-WT3	41.78	3062.0	3.38
ID3-WT7	41.40	3155.0	3.40
ID7-WT3	42.10	3180.0	3.13
ID7-WT7	44.80	3217.5	3.68

According to the values in Table 4, with the increase of the distance between the parts from 3 mm to 7 mm, an increase in the flex modulus and flexural strength was observed. The increase in the wall thickness of the neighboring part also increased these values. There is no evident change seen at the elongation percentages with increasing wall thickness or distance between parts.

The variation of the flexural modulus and flexural strength according to the exposed temperature is shown in Figure 47 and 48 respectively. The decrease in the exposed temperature caused an increase in the flexural strength and modulus of the part.

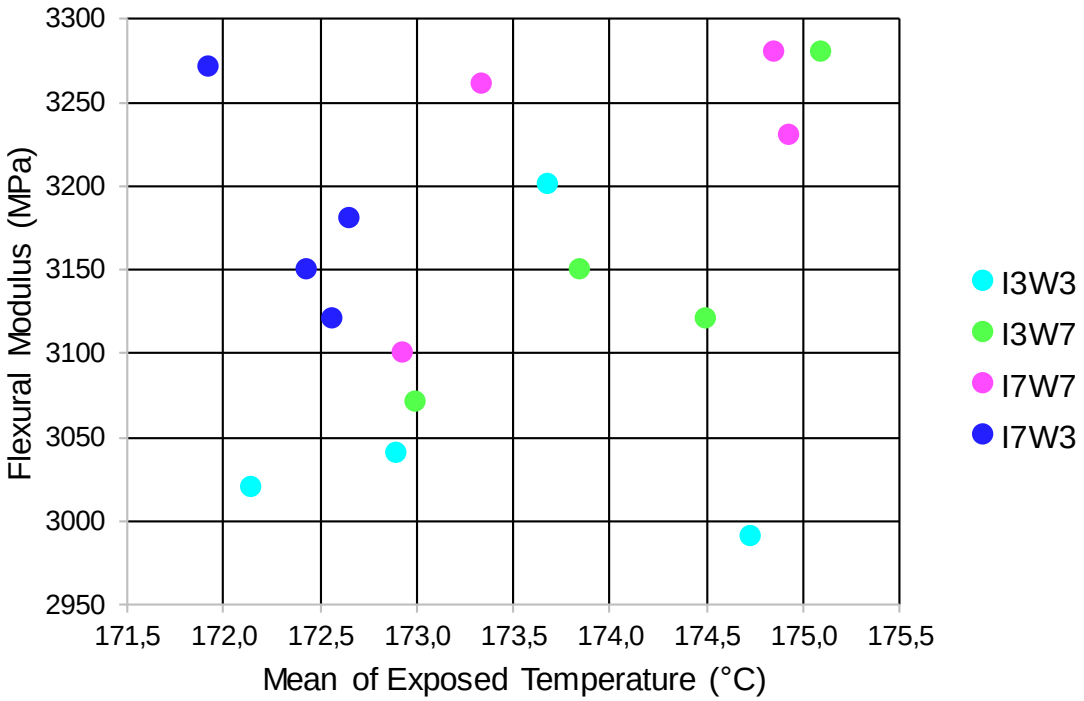

Figure 47 The effect of the temperature exposed to the bending sample on the flexural modulus

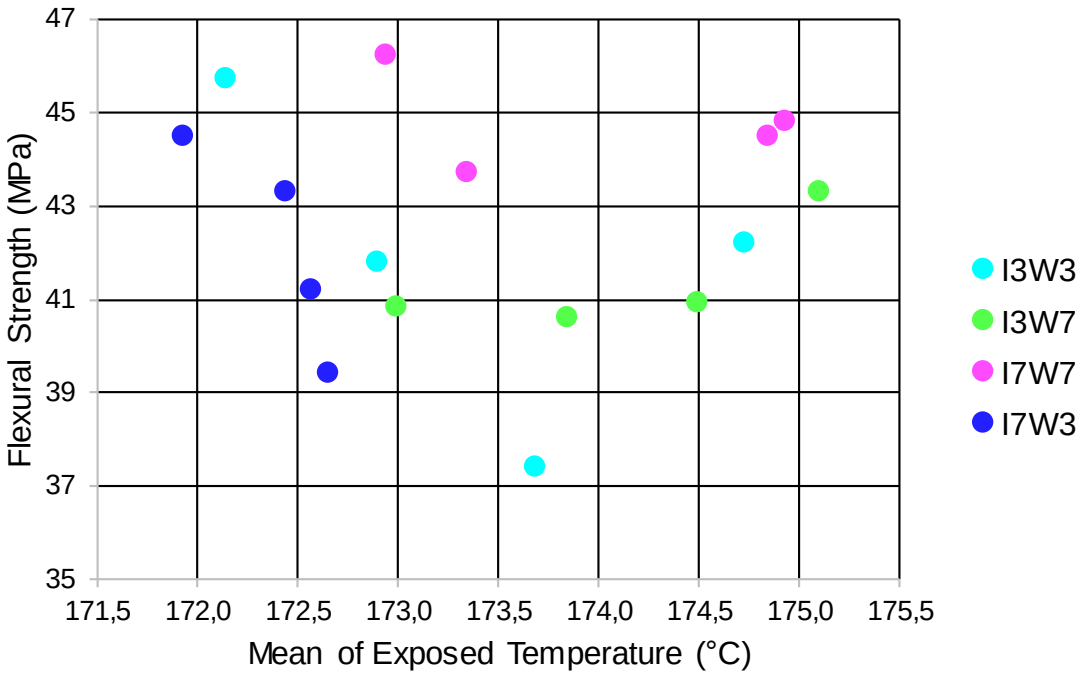

Figure 48 The effect of the temperature exposed to the bending sample on the flexural strength

5.4. DSC Quantification

DSC analysis were performed using Mettler Toledo 821e equipment (Figure 49) and STARe software. Samples were heated from 25 °C to 220 °C at a rate of 10 °C/min then, cooled at the same rate from 220 °C to 20 °C. Melting and crystallization temperatures, T_m and T_c respectively, were obtained from DSC thermograms. The degree of crystallinity was calculated using the melting enthalpy obtained by integrating the area under the melting peak. Equation 4 in Section 2.3.2 is used. DSC analysis has done for both powder and bending samples. Three replicates were performed for each sample type.

Figure 49 Mettler Toledo DSC821e, heat-flux type DSC

Table 5 and Table 6 presents the results of the DSC analysis for powder and the bending specimen respectively. In the section "2.3.2. Material Testing Methods", the descriptions of the values are available. "Sintering window" of the powder in Table 5 is calculated by extracting crystallization onset from melting onset temperature, $T_{c,onset}$ and $T_{m,onset}$ respectively. The melting and crystallization ranges, ΔT_m and ΔT_c respectively, are the difference of onset and endset temperatures of each transition temperature. When material reach at the $T_{m,endset}$, melting endset temperature, material state is totally melted. For $T_{c,endset}$, crystallization endset temperature, the values which reflect the mean values of replicates for each sample were selected and used.

Table 5 Thermal properties of the powders obtained from DSC analysis

Sample	Tm (°C)	Tc (°C)	ΔTm (°C)	ΔTc (°C)	ΔHc (mJ/mg)	ΔHf (mJ/mg)	Sintering Window (°C)	χ
VIRGIN	189.9	150.0	10.0	10.8	24.9	35.5	29.6	17.0
BOX	191.7	146.5	14.1	13.1	21.0	27.7	28.9	13.2
ID7-WT3	192.3	146.1	15.4	13.4	19.8	27.8	29.9	13.3
ID7-WT7	192.1	146.1	15.5	13.4	15.1	21.7	29.6	10.4
ID3-WT3	192.3	145.9	14.6	13.9	27.4	33.0	30.9	15.8
ID3-WT7	191.9	146.4	13.8	13.0	23.2	26.8	29.8	12.8

Table 6 Thermal properties of the bending parts obtained from DSC analysis

Sample	Tm (°C)	Tc (°C)	ΔTm (°C)	ΔTc (°C)	ΔHc (mJ/mg)	ΔHf (mJ/mg)	χ
ID7-WT3	191.6	146.5	18.5	12.8	19.4	15.1	7.2
ID7-WT7	191.1	146.4	19.1	12.9	18.6	13.6	6.5
ID3-WT3	191.6	146.6	18.3	12.4	19.8	14.8	7.1
ID3-WT7	191.3	146.2	18.2	13.0	18.9	14.5	6.9

In the analysis results of the powders, there was no difference found between the sintering windows of the samples. No major differences were observed between the crystallization interval and the crystallization peaks (Table 5). The difference between the melting peaks are also very low, but the melting limits differ from each other. Increasing the distance between the pieces from 3mm to 7mm has extended the melting range of the powder. The change in wall thickness did not affect the melting range of the powder. Increasing the wall thickness from 3mm to 7mm and the inter-part distance from 3 mm to 7 mm caused a decrease in crystallization and melting enthalpies. The percentage of crystallinity (χ) decreased with increasing wall thickness and inter-part distance. As a result of the DSC tests on the bending samples, the distance between the parts did not show any effect, but

with the increase in the wall thickness the melting range increased. Whereas, the melting and crystallization enthalpies and the percentage of crystallinity decreased. Looking at the DSC thermogram in Figure 50, it is seen that the melting and crystallization regions of the virgin powder are narrow and deep. An increase in the melting peak (Figure 52) and a decrease in the crystallization peak (Figure 51) were observed in all sample powders.

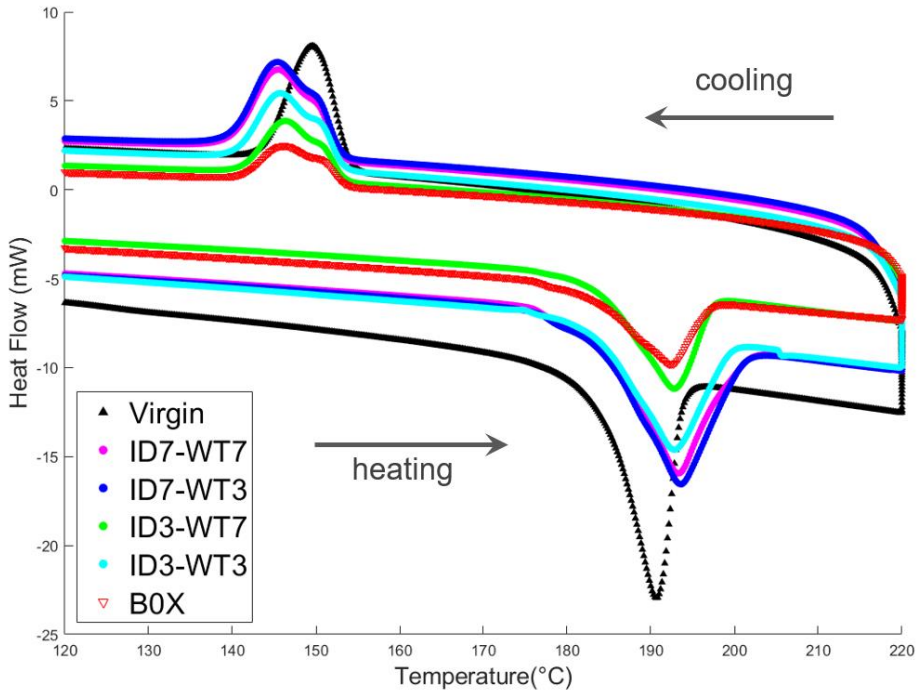

Figure 50 Influence of the nesting parameters on thermal properties of glass filled polyamide 12 powder

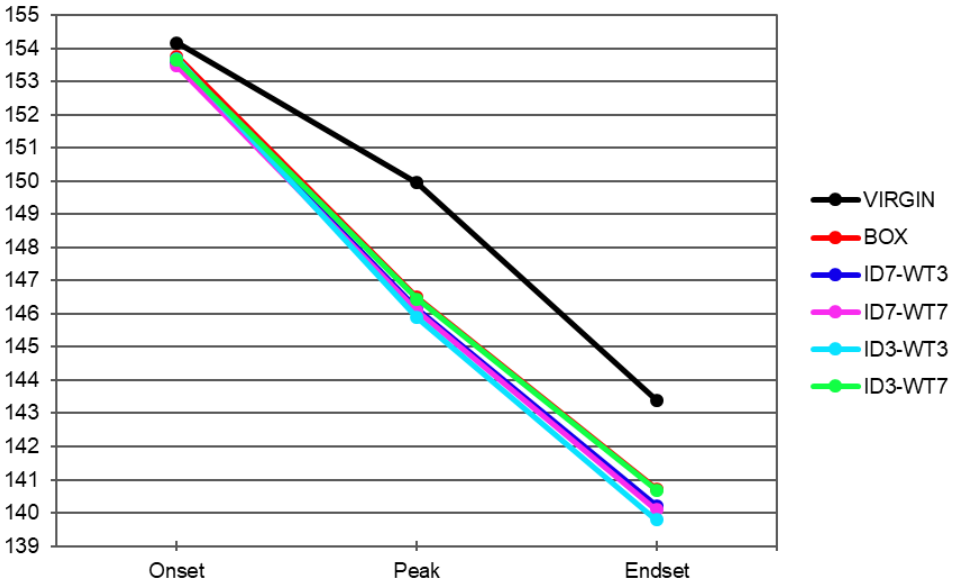

Figure 51 Crystallization temperature results from DSC analysis of powders

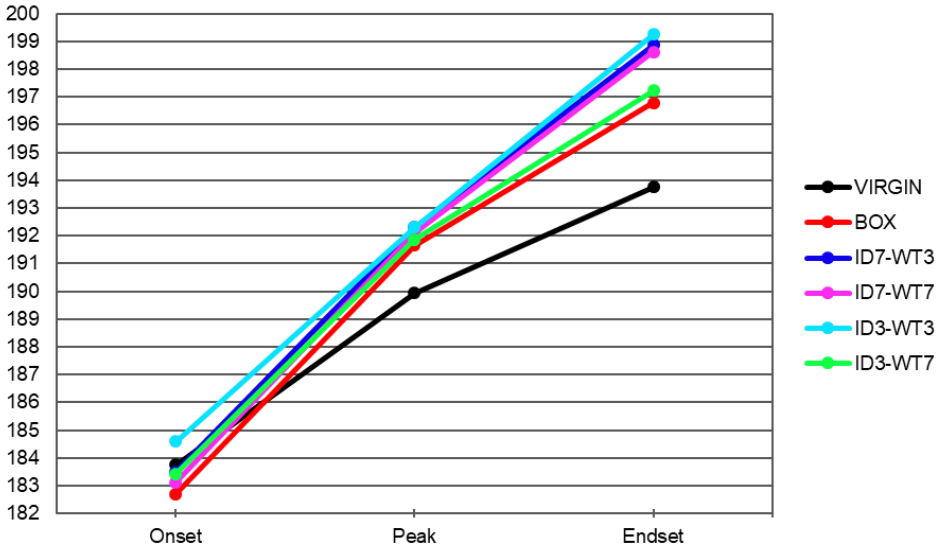

Figure 52 Melting temperature results from DSC analysis of powders

CHAPTER 6 CONCLUSION

SLS is a process based on the interaction of the material with temperature. Usually 5-10% by volume of the raw material is used for building parts, the rest is non-sintered powder. The powder, which is compacted on the build platform, serves as a support for the sintered parts and thus the parts can be positioned freely up to the production height of the machine. While arranging the build plan in software, the minimum distance value between the parts to be placed on the platform is determined by the user. If this distance value is decreased, the same number of parts will have a lower production height as the parts will be positioned closer to each other and thus parts can be produced in a shorter time. However, in industrial applications, it has been experienced that when the parts come closer to each other, cool-down of the build cake becomes longer and sometimes powder aggregates are observed. The process temperatures are very close to the melting temperature of the material, hence the powder material deteriorates over time under the influence of the temperature. Since the non-sintered powder from the build cake is the raw material mixture of the next build, the thermal and chemical properties of the powder are very important. If the un-sintered powder, which constitutes 80-90% of the build cake, was exposed to temperature uncontrolled, it may become unusable and causing significant environmental and financial loss. In the SLS method, many information about the process and produced parts can be obtained by thermal imaging. In previous studies, process parameters and part geometry have been shown to affect the time-temperature story in the. However, it has not been investigated how the distance between the parts used in the production plan affects the process. In order to answer this question, an innovative sample set was designed in this thesis and the temperatures of the parts in the process were measured using thermal imaging. The bending test of the produced parts and the DSC analysis of the un-sintered powder were performed. Unlike thermal imaging systems used in previous studies, a new system has been developed that can be used without disrupting

the structure of the SLS machine. The system installed just by screwing it by utilizing the laser window holding unit. Because of using Sinterstation 2500 Plus's own air compressor, there is no additional investment required for the cooling system. Low cost kit has been developed. Only a certain part of the production could be evaluated due to the condensation on the window of the housing. The reason and solution ways of condensation were investigated and future studies were mentioned.

During exposing to heat, the time that exposed to heat is as important as temperature. Temperature distribution charts have been created to show the exposure ranges and times. It was observed that the temperature of the sintered part increased with increasing wall thickness and decreasing the distance between the parts. As in the literature, an increase in the temperature of the wall was observed as the wall thickness increased. As the inter-part distance decreased, the temperature of the powder increased inversely. It has been confirmed that the wall thickness of the adjacent part is also an important factor affecting the temperature of the bending part. The flexural modulus and strength increased with the increase of the distance between the parts and the wall thickness of the adjacent part. When looking at the thermography results, the reason for the increase in strength and modulus in line with the information obtained from the temperature distribution graphics can be attributed to the increase in temperature. With the DSC tests performed, it was observed that there was a decrease in the crystallinity of the powder between the parts, and this is due to the higher temperature it is exposed to.

It was understood from the results of DSC and three-point bending tests that the distance between the parts and the wall thickness of the adjacent part affect the mechanical properties of the part and the thermal and chemical properties of the powder in between. In line with the thermography results, changes were observed in powder and parts due to the temperature-time history. It is understood that with the help of thermal imaging, interpretation can be made about the properties of the powder and the parts during the SLS process.

CHAPTER 7 FUTURE WORK

The feasibility of the newly developed thermal camera kit within the machine has been approved with the work done in this thesis study. It is planned to design a system that will create a gas curtain by blowing nitrogen in front of the glass to prevent condensation on the glass of the enclosure after a certain period of time. It has been demonstrated that the low-cost uncooled microbolometer type LWIR camera module is sufficient to analyze process temperatures. However, it is planned to use a higher resolution model for small-size defect detection and temperature analysis of smaller regions across the powder bed. As a result of experimental studies, it has been shown that the nesting factor has an effect on the properties of the non-sintered powder and the sintered part. In the future studies, it is planned to examine the effect of the powder mixture used for production on the nesting factors.

REFERENCES

[1] S. Fish, J.C. Booth, S.T. Kubiak, W.W. Wroe, A.D. Bryant, D.R. Moser, J.J. Beaman, Design and subsystem development of a high temperature selective laser sintering machine for enhanced process monitoring and control, Addit. Manuf. 5 (2015) 60–67. https://doi.org/10.1016/j.addma.2014.12.005.

[2] M. Abdelrahman, T.L. Starr, Layerwise monitoring of polymer Laser Sintering using thermal imaging, Proc. Solid Free. Fabr. Symp. Austin, Texas. (2014) 244–255.

[3] T. Phillips, S. Fish, J. Beaman, Development of an automated laser control system for improving temperature uniformity and controlling component strength in selective laser sintering, Addit. Manuf. 24 (2018) 316–322. https://doi.org/10.1016/j.addma.2018.10.016.

[4] W.W. Wroe, Improvements and effects of thermal history on mechanical properties for polymer selective laser sintering (SLS), University of Texas at Austin, 2015.

[5] I. Campbell, D. Bourell, I. Gibson, Additive manufacturing: rapid prototyping comes of age, Rapid Prototyp. J. 18 (2012) 255–258. https://doi.org/10.1108/13552541211231563.

[6] B. Gibson, I.; Rosen, D. W.; Stucker, Additive Manufacturing Technologies, 2010. https://doi.org/10.1007/978-1-4419-1120-9.

[7] L. Columbus, The State of 3D Printing, Forbes. (2017) 26. https://www.forbes.com/sites/louiscolumbus/2017/05/23/the-state-of-3d-printing-2017/#4fad87db57eb.

[8] G. Flodberg, H. Pettersson, L. Yang, Pore analysis and mechanical performance of selective laser sintered objects, Addit. Manuf. 24 (2018) 307–315. https://doi.org/10.1016/j.addma.2018.10.001.

[9] ASTM International, F2792-12a - Standard Terminology for Additive Manufacturing Technologies, Rapid Manuf. Assoc. (2013) 10–12. https://doi.org/10.1520/F2792-12A.2.

[10] M. Schmid, Laser Sintering with Plastics: Technology, Processes, and Materials, Hanser Publications, 2018.

[11] K. Dotchev, W. Yusoff, Recycling of polyamide 12 based powders in the laser sintering process, Rapid Prototyp. J. 15 (2009) 192–203. https://doi.org/10.1108/13552540910960299.

[12] C. Reiff, F. Wulle, O. Riedel, S. Epple, V. Onuseit, On inline process control for selective laser sintering, 8th Int. Conf. Mass Cust. Pers. – Community Eur. (MCP-CE 2018). (2018) 230–239.

[13] S. Rüsenberg, S. Josupeit, H. Schmid, A Method to Characterize the Quality of a Polymer Laser Sintering Process, 2014 (2014). https://doi.org/10.1155/2014/185374.

[14] H.J. O' Connor, D.P. Dowling, Comparison between the properties of polyamide

12 and glass bead filled polyamide 12 using the multi jet fusion printing process, Addit. Manuf. 31 (2020) 100961. https://doi.org/10.1016/j.addma.2019.100961.

[15] Materialise, Materialise Magics User Manual, 3001 Leuven, Belgium, n.d.

[16] W. A, Wegner; G, PROCESS MONITORING IN LASER SINTERING USING THERMAL IMAGING, in: 22nd Annu. Int. Solid Free. Fabr. Symp. - An Addit. Manuf. Conf. SFF 2011, 2011: pp. 405–414.

[17] K. Wudy, D. Drummer, Aging e ff ects of polyamide 12 in selective laser sintering : Molecular weight distribution and thermal properties, Addit. Manuf. 25 (2019) 1–9. https://doi.org/10.1016/j.addma.2018.11.007.

[18] D.T. Pham, K.D. Dotchev, W.A.Y. Yusoff, Deterioration of polyamide powder properties in the laser sintering process, Proc. Inst. Mech. Eng. Part C J. Mech. Eng. Sci. 222 (2008) 2163–2176. https://doi.org/10.1243/09544062JMES839.

[19] M. Schmid, K. Wegener, Additive Manufacturing: Polymers applicable for laser sintering (LS), Procedia Eng. 149 (2016) 457–464. https://doi.org/10.1016/j.proeng.2016.06.692.

[20] W.D. Callister, Materials Science and Engineering: an Introduction, 2006.

[21] A.J. Cano, A. Salazar, J. Rodríguez, Effect of temperature on the fracture behavior of polyamide 12 and glass-filled polyamide 12 processed by selective laser sintering, Eng. Fract. Mech. 203 (2018) 66–80. https://doi.org/10.1016/j.engfracmech.2018.07.035.

[22] M.I. Kohan, Nylon Plastics Handbook, Hanser Publications, New York, 1995.

[23] R.D. Goodridge, C.J. Tuck, R.J.M. Hague, Laser sintering of polyamides and other polymers, Prog. Mater. Sci. 57 (2012) 229–267. https://doi.org/10.1016/j.pmatsci.2011.04.001.

[24] J. Kim, T.S. Creasy, Selective laser sintering characteristics of nylon 6/clay-reinforced nanocomposite, Polym. Test. 23 (2004) 629–636. https://doi.org/10.1016/j.polymertesting.2004.01.014.

[25] S. Ruesenberg, H. Schmid, Advanced characterization method of nylon 12 materials for application in laser sinter processing Advanced Characterization Method of Nylon 12 Materials for Application in Laser Sinter Processing, 713 (2016). https://doi.org/10.1063/1.4873877.

[26] S. Dadbakhsh, L. Verbelen, O. Verkinderen, D. Strobbe, P. Van Puyvelde, J.P. Kruth, Effect of PA12 powder reuse on coalescence behaviour and microstructure of SLS parts, Eur. Polym. J. 92 (2017) 250–262. https://doi.org/10.1016/j.eurpolymj.2017.05.014.

[27] L. Verbelen, S. Dadbakhsh, M. Van Den Eynde, J.P. Kruth, B. Goderis, P. Van Puyvelde, Characterization of polyamide powders for determination of laser sintering processability, Eur. Polym. J. 75 (2016) 163–174. https://doi.org/10.1016/j.eurpolymj.2015.12.014.

[28] G. Craft, J. Nussbaum, N. Crane, J.P. Harmon, Impact of extended sintering times on mechanical properties in PA-12 parts produced by powderbed fusion processes, Addit. Manuf. 22 (2018) 800–806.

https://doi.org/10.1016/j.addma.2018.06.028.

[29] R. Seltzer, F.M. de la Escalera, J. Segurado, Effect of water conditioning on the fracture behavior of PA12 composites processed by selective laser sintering, Mater. Sci. Eng. A. 528 (2011) 6927–6933. https://doi.org/10.1016/j.msea.2011.05.045.

[30] Y. Kong, J.N. Hay, The enthalpy of fusion and degree of crystallinity of polymers as measured by DSC, Eur. Polym. J. 39 (2003) 1721–1727. https://doi.org/10.1016/S0014-3057(03)00054-5.

[31] M. Schmid, K. Wegener, Additive Manufacturing : Polymers applicable for Laser Sintering (LS), Procedia Eng. 149 (2016) 457–464. https://doi.org/10.1016/j.proeng.2016.06.692.

[32] M. Yuan, D. Bourell, Efforts to Reduce Part Bed Thermal Gradients during Laser Sintering Processing, Solid Free. Fabr. Symp. (2012) 962–974.

[33] T.T. Diller, R. Sreenivasan, J. Beaman, D. Bourell, J. Larocco, Thermal model of the build environment for polyamide powder selective laser sintering, 21st Annu. Int. Solid Free. Fabr. Symp. - An Addit. Manuf. Conf. SFF 2010. (2010) 539–548.

[34] H. Krauss, C. Eschey, M.F. Zaeh, Thermography for Monitoring the SLM Process, 23rd Annu. Int. Solid Free. Fabr. Symp. - An Addit. Manuf. Conf. SFF 2012. 66 (2012) 999–1014.

[35] M. Abdelrahman, T.L. Starr, Feedforward Control for Polymer Laser Sintering Process Using Part Geometry, Solid Free. Fabr. Symp. 91 (2015) 492–500. https://doi.org/10.1017/CBO9781107415324.004.

[36] T.A. Morris, M.A. Marciniak, G.C. Wollenweber, J.A. Turk, Analysis of uncertainties in infrared camera measurements of a turbofan engine in an altitude test cell, Infrared Phys. Technol. 48 (2006) 130–153. https://doi.org/10.1016/j.infrared.2005.07.001.

[37] B.H. Burzlaff, J.S. Chivian, W.D. Cotten, R.B. Hemphill, M.A. Huhlein, Active two-phase cooling of an ir window for a hypersonic interceptor, 2nd AIAA SDIO Annu. Intercept. Technol. Conf. 1993. (1993). https://doi.org/10.2514/6.1993-2685.

[38] EN ISO 178, Plastics - Determination of flexural properties, (2019).

[39] D. Sassaman, P. Hall, S. Fish, J. Beaman, Two-Dimensional Characterization of Window Contamination in Selective Laser Sintering, (2018) 2305–2314.

[40] B. Fulcher, D.K. Leigh, EFFECTS OF LASER WINDOW DEGREDATION ON LASER POWER AND, (n.d.) 150–161.

[41] J.P. Partanen, Z. Ning, R.J. Bishop, LASER SINTERING PROCESS CHAMBER GAS CURTAIN WINDOW CLEANSING IN ALASER SINTERING SYSTEM, US 7,807,947 B2, 2010.